

RESEARCH

Open Access



AXL promotes inflammatory breast cancer progression by regulating immunosuppressive macrophage polarization

Lan T. H. Phi^{1,2†}, Yating Cheng^{1†}, Yohei Funakoshi^{1†}, Francois Bertucci^{3,4}, Pascal Finetti³, Steven J. Van Laere⁵, Fang Zou¹, James P. Long⁶, Suguru Ogata^{7,8}, Savitri Krishnamurthy⁹, James M. Reuben¹⁰, Jason M. Foulks¹¹, Steven L. Warner¹¹, Jennifer M. Rosenbluth¹², Anil K. Sood¹³, Debu Tripathy¹, Naoto T. Ueno^{1,7,8*} and Xiaoping Wang^{1,7,8*}

Abstract

Background Tumor-associated macrophages (TAMs) are key promoters of inflammatory breast cancer (IBC), the most aggressive form of breast cancer. The receptor tyrosine kinase AXL is highly expressed in various cancer types, including IBC, but its role in TAMs remains unexplored.

Methods We examined the effects of AXL inhibitor TP-0903 on tumor growth and tumor microenvironment (TME) component M2 macrophages (CD206⁺) in IBC and triple-negative breast cancer mouse models using flow cytometry and immunohistochemical staining. Additionally, we knocked out AXL expression in human THP-1 monocytes and evaluated the effect of AXL signaling on immunosuppressive M2 macrophage polarization and IBC cell growth and migration. We then investigated the underlying mechanisms through RNA sequencing analysis. Last, we performed CIBERSORT deconvolution to analyze the association between AXL expression and tumor-infiltrating immune cell types in tumor samples from the Inflammatory Breast Cancer International Consortium.

Results We found that inhibiting the AXL pathway significantly reduced IBC tumor growth and decreased CD206⁺ macrophage populations within tumors. Mechanistically, our in vitro data showed that AXL promoted M2 macrophage polarization and enhanced the secretion of immunosuppressive chemokines, including CCL20, CCL26, and epiregulin, via the transcription factor STAT6 and thereby accelerated IBC cell growth and migration. RNA sequencing analysis further indicated that AXL signaling in immunosuppressive M2 macrophages regulated the expression of molecules and cytokines, contributing to an immunosuppressive TME in IBC. Moreover, high AXL expression was correlated with larger populations of immunosuppressive immune cells but smaller populations of immunoreactive immune cells in tissues from patients with IBC.

Conclusions AXL signaling promotes IBC growth by inducing M2 macrophage polarization and driving the secretion of immunosuppressive molecules and cytokines via STAT6 signaling, thereby contributing to an immunosuppressive

[†]Lan T. H. Phi, Yating Cheng and Yohei Funakoshi have contributed equally to this work.

*Correspondence:

Naoto T. Ueno

nueno@cc.hawaii.edu

Xiaoping Wang

xiaopingwang@cc.hawaii.edu

Full list of author information is available at the end of the article



TME. Collectively, these findings highlight the potential of targeting AXL signaling as a novel therapeutic approach for IBC that warrants further investigation in clinical trials.

Introduction

Inflammatory breast cancer (IBC) is the most lethal and aggressive form of breast cancer, accounting for 2–4% of breast cancer cases but 8–10% of breast cancer deaths [1, 2]. Despite IBC's aggressiveness, therapeutic approaches specific for IBC are lacking, underscoring the urgent need for novel therapeutic targets to improve the treatment of IBC.

Therapies targeting the tumor microenvironment (TME) have shown promise in improving patient outcomes [3]. Recent studies have revealed the crucial role of the TME in the pathogenesis and aggressiveness of IBC [4]. Among immune cell components in the TME, tumor-associated macrophages (TAMs) play pivotal roles in promoting tumor initiation and metastasis [5], suppressing T cell-mediated anti-tumor immune responses [6], stimulating tumor angiogenesis [7], and thus leading tumor progression [8]. TAMs typically exhibit the M2 phenotype, which promotes tumor growth [9]. In IBC patients, TAMs are critical drivers of the IBC growth and enhance metastasis [10], with high infiltration of M2 macrophages being a hallmark of IBC [11]. Recent reports reveal that IBC may promote the development of M2 macrophages and mesenchymal cancer cells via a complex cytokine network [11], highlighting the importance of targeting M2 macrophages as a therapeutic strategy for patients with IBC.

AXL, a receptor tyrosine kinase, plays essential roles in promoting various cancers, including lung [12] and breast [13] cancer. AXL overexpression in cancer cells is linked to epithelial-to-mesenchymal transition [14], tumor angiogenesis [15], and resistance to chemotherapy and targeted therapies [16]. Moreover, high AXL expression is associated with reduced survival in triple-negative breast cancer (TNBC) patients [17]. Targeting AXL signaling with TP-0903, a selective AXL inhibitor, has shown promise in preclinical models by inhibiting tumor growth and overcoming drug resistance for several types of cancers [18, 19]. TP-0903 was evaluated in phase 1 clinical trials for various advanced solid tumors (NCT02729298), chronic lymphocytic leukemia (NCT03572634), and *FLT3* gene-mutated acute myeloid leukemia (NCT04518345) [20]. Furthermore, AXL signaling is associated with decreased anti-tumor responses by immune cells, including tumor stromal cells [21] and M2 macrophages [22, 23]. However, the role of AXL signaling in the TAMs of IBC patients is unknown.

Given the pivotal role of AXL signaling in cancer progression and AXL's potential as a therapeutic target, we hypothesized that AXL promotes IBC aggressiveness via modulating the responses of multiple immune cell types in the IBC TME, particularly through direct effects on M2 macrophages. To test this hypothesis, we investigated AXL's dual biological functions in IBC cells and immunosuppressive M2 macrophages, and we explored how AXL modulates the interplay of IBC cells and M2 macrophages to elucidate the role of AXL signaling in IBC progression.

Methods

Cell lines

The human IBC cell line SUM149 was purchased from Asterand (Detroit, MI), and the human IBC cell line BCX010 was provided by Dr. Funda Meric-Bernstam (The University of Texas MD Anderson Cancer Center). Both cell lines were grown in Ham's F12 medium supplemented with 5% fetal bovine serum (FBS), 5 µg/ml insulin, 1 µg/ml hydrocortisone, and 1% antibiotic-antimycotic in a 5% CO₂ atmosphere at 37 °C. 4T1.2 murine TNBC cells were obtained from Robin L. Anderson (School of Cancer Medicine, La Trobe University, Melbourne, Australia), and E0771 murine TNBC cells were purchased from CH3 BioSystems (Amherst, NY). THP-1 acute monocytic leukemia cells were purchased from the ATCC (Manassas, VA). 4T1.2, E0771, and THP-1 cells were cultured in RPMI 1640 medium supplemented with 10% FBS and 1% antibiotic-antimycotic in a 5% CO₂ atmosphere at 37 °C. Cell lines were authenticated at the MD Anderson Cytogenetics and Cell Authentication Core facility using a short tandem repeat method that is based on primer extension and detects single-base deviations.

Materials

TP-0903 was provided by Sumitomo Pharma America, Inc. (formerly known as Sumitomo Pharma Oncology, Inc.) (Marlborough, MA). Phorbol 12-myristate 13-acetate (PMA) (1652981) and recombinant human proteins, including MIP-3α (CCL20; 300-29A), eotaxin-3 (CCL26; 300-48), epiregulin (EREG; 100-04), interleukin (IL)-4 (200-04), and IL-13 (200-13), were purchased from PeproTech (Cranbury, NJ).

Small interfering RNAs (siRNAs) targeting STAT6 (SASI_Hs01_00228593 and SASI_Hs01_00228594) and a scrambled control siRNA (MISSION siRNA

Universal Negative Control #1; SIC001) were purchased from Sigma-Aldrich (Burlington, MA). Lipofectamine RNAiMAX Transfection Reagent (13778150) and Lipofectamine CRISPRMAX Cas9 Transfection Reagent (CMAX00003) were purchased from Invitrogen (Waltham, MA). AXL sequence-specific CRISPR RNA (Hs.Cas9.AXL.1.AA—rUrG rCrGrA rArGrC rCrCrA rUrArA rCrGrC rCrArA rGrUrU rUrUrA rGrArG rCrUrA rUrGrC rU), transactivating RNA (1072533), and recombinant Alt-R S.p. Cas9 Nuclease V3 (1081058) were obtained from Integrated DNA Technologies (Coralville, IA) to generate a Cas9 ribonucleoprotein complex. To generate STAT6-overexpressing cells, a LentiORF clone of human Myc-DDK-tagged STAT6 (RC210065L3) was purchased from OriGene (Rockville, MD). Opti-MEM (Thermo Fisher Scientific, Waltham, MA; 31-985-070) and FuGENE HD (Promega, Madison, WI; E2311) were used for cell transfection of this STAT6 plasmid.

Ultra-low attachment six-well plates (Corning, Corning, NY; 3471) and a MammoCult human medium kit (STEMCELL Technologies, Vancouver, BC; 05620) were used for a mammosphere formation assay. A CellTiter-Blue (CTB) cell viability assay kit (Promega; G8081) was used for a cell growth assay. Falcon cell culture inserts with 8- μ m pore size (Corning; 353097) were used for a migration assay.

A PureLink RNA Mini Kit (Thermo Fisher Scientific; 12183018A), amfiRivert cDNA Synthesis Platinum Master Mix (GenDEPOT, Barker, TX; R5600), and iTaq Universal SYBR Green Supermix (Bio-Rad, Hercules, CA; 1725121) were used for quantitative reverse transcription-polymerase chain reaction (qRT-PCR) analysis. A protease inhibitor and phosphatase inhibitor cocktail (Bimake.com, Houston, TX; B14001 and B15001), NuPAGE LDS Sample Buffer (Thermo Fisher Scientific; NP0007), 12% NuPAGE Bis-Tris gels (Thermo Fisher Scientific; NP0322), and an Immun-Blot polyvinylidene fluoride membrane (Bio-Rad; 1620177) were used for cell lysis, gel running, and membrane transfer. The following primary antibodies were used for Western blotting: anti-human phospho-AXL ([Y779] R&D Systems, Minneapolis, MN; AF2228), anti-human AXL (Sigma; WH0000558M1), anti-mouse AXL (R&D Systems; AF854), anti-human phospho-STAT6 ([Tyr641] Cell Signaling Technology, Danvers, MA; 56554S), anti-human STAT6 (Cell Signaling Technology; 9362S), anti-human CD206 (R&D Systems; MAB25341), and anti-human β -Actin (Sigma; A5316). Horseradish peroxidase-conjugated anti-rabbit (31460), anti-goat (A16005), and anti-mouse (31430) antibodies were purchased from Invitrogen and used as secondary antibodies. HyBlot CL autoradiography film (Thomas Scientific, Chadds Ford Township, PA; 1141J52), Pierce ECL Western Blotting

Substrate (Thermo Fisher Scientific; 32106), SuperSignal West Dura Extended Duration Substrate (Thermo Fisher Scientific; 34075), and a Mini-Med 90 X-ray film processor (AFP Manufacturing, Peachtree City, GA) were used for detection of specific proteins. Human CCL20 (DY360), CCL26 (DCC260B), EREG (DY1195), CXCL9 (DY392), and CXCL10 (DY266) DuoSet enzyme-linked immunosorbent assay (ELISA) kits were purchased from R&D Systems and used for protein level measurement. A VICTOR X plate reader (PerkinElmer, Waltham, MA) was used to determine the optical density of specific proteins.

A Matrigel membrane matrix (Corning; CB-40234) was used for inoculating cells into mice. A human/mouse tumor dissociation kit (Miltenyi Biotec, Bergisch Gladbach, Germany; 130-095-929/130-096-730), 40 μ m cell strainers (Falcon; 352340), and red blood cell lysis buffer (Sigma; 11814389001) were used to generate single cell suspensions from tumor tissues for flow cytometric analysis.

The following mouse antibodies were used in flow cytometry for analyzing mouse CD206⁺ macrophages (CD45⁺CD11b⁺Ly6C⁻Ly6G⁻F4/80⁺CD206⁺) in SUM149 and 4T1.2 mouse models and mouse immunosuppressive regulatory T cells (Tregs) (CD45⁺CD3⁺CD4⁺CD25⁺FOXP3⁺) in the 4T1.2 mouse model: CD45-FITC (BioLegend, San Diego, CA; 103108), CD11b-PE/Dazzle 594 (BioLegend; 101256), Ly6C-Pacific Blue (BioLegend; 128014), Ly6G-PerCP/Cy5.5 (BioLegend; 127616), F4/80-APC/Fire 750 (BioLegend; 123151), CD206-APC (BioLegend; 141708), CD3-PerCP/Cy5.5 (BioLegend; 100217), CD4-Pacific Blue (BioLegend; 100531), CD25-APC/Fire 750 ([PC61] BioLegend; 102054), and FOXP3-PE Cy7 (eBioscience, San Diego, CA; 25-5773-82). Also, the mouse antibodies CD45-FITC, CD11b-PE (BioLegend; 101208), F4/80-Alexa700 (BioLegend; 123130), Ly6C-Pacific Blue, Ly6G-PerCP/Cy5.5, CD3-PerCp (BioLegend; 100218), CD4-APC (BioLegend; 100412), CD25-APC/Fire 750, and FOXP3-PE Cy7 were used in flow cytometry for analyzing mouse macrophages (CD45⁺CD11b⁺F4/80⁺Ly6C⁻Ly6G⁻) and Tregs (CD45⁺CD3⁺CD4⁺CD25⁺FOXP3⁺) in the E0771 mouse model. In addition, the primary human antibodies CD68-PerCP/Cy5.5 (BioLegend; 333814), CD163-PE (BioLegend; 155308), and CD206-APC/Cy7 (BioLegend; 321120) were used in flow cytometry for analyzing M2 macrophages (CD68⁺CD163⁺CD206⁺) polarized from THP-1 cells. LIVE/DEAD Fixable Aqua Dead Cell Stain Kit (Thermo Fisher Scientific; L34957) was used to identify live cells.

For histological analysis of tumor tissues, 10% neutral buffered formalin (28600-1) was purchased from

StatLab Medical Products (McKinney, TX) and used to fix tumor tissues and create tissue blocks. AR6 buffer (Akoya Biosciences, Marlborough, MA; AR600125), a 30% hydrogen peroxide solution (w/w) in water (Sigma; H1009), a VECTASTAIN Elite ABC-HRP universal kit (Vector Laboratories, Newark, CA; PK7200), 3,3'-diaminobenzidine (Vector Laboratories; SK4100), a hematoxylin solution (Vector Laboratories; H3404), Permount mounting medium (Thermo Fisher Scientific; SP15100), human (MAB25341) and mouse MMR/CD206 antibodies (R&D Systems; AF2535), and biotinylated rabbit anti-goat IgG ([H+L] Vector Laboratories; BA-5000-1.5) were used for immunohistochemical staining.

Macrophage polarization

THP-1 cells (1×10^6) were plated in a 10 cm cell culture dish with RPMI 1640 medium supplemented with 10% FBS and 100 ng/ml PMA overnight to differentiate them into M0 macrophages. To generate M2 macrophages, M0 macrophages were incubated with RPMI 1640 medium supplemented with 10% FBS, 20 ng/ml IL-4, and 20 ng/ml IL-13 for 48 h.

SiRNA transfection assay

THP-1 cells were transfected with siRNAs using Lipofectamine RNAiMAX Transfection Reagent following the manufacturer's instructions (Invitrogen). After 72 h of transfection, cells were polarized into M2 macrophages and harvested for further analysis.

Generation of stable knockout (KO) and STAT6-overexpressing cells

The bimolecular guide RNA was incubated with recombinant Alt-R S.p. Cas9 Nuclease V3 to form the Cas9 ribonucleoprotein complex for transfection using Lipofectamine CRISPRMAX Cas9 Transfection Reagent according to the manufacturer's instructions (Integrated DNA Technologies). Transfected THP-1 cells were then expanded, and KO of AXL was verified by Western blotting.

To generate STAT6-overexpressing cells, 2×10^6 THP-1 cells were plated in a six-well plate with fresh growth medium without antibiotic-antimycotic and grew overnight to reach 70–80% confluence. The cells were then transfected with 100 μ l of Opti-MEM containing 3 μ l of FuGENE HD and 1 μ g of human Myc-DDK-tagged STAT6 (RC210065L3) according to the manufacturer's instructions (Promega). Cells were harvested for further analysis after 48 h of transfection.

Mammosphere formation assay

Primary and secondary mammospheres of IBC cells, including SUM149 and BCX010 cells, were cultured in ultra-low attachment six-well plates using a MammoCult human medium kit including basal medium supplemented with proliferation supplements, 0.48 μ g/ml hydrocortisone, and 4 μ g/ml heparin for 7 days. Cells were seeded at densities of 20,000 per well for primary mammosphere formation and 10,000 per well for secondary mammosphere formation, as described previously [24]. Spheres were stained with MTT (0.4 mg/ml), and the spheres larger than 80 μ m were quantified using GelCount scanning software (Oxford Optronix, Oxford, UK).

Cell growth assay

Cancer cells were plated in 96-well plates overnight (4×10^3 SUM149 cells or 2×10^3 BCX010 cells per well). The media were then replaced with 100% conditioned medium (CM) collected from AXL-KO or TP-0903-treated M2 macrophages and control clones after 48 h of culture, and the cancer cells were incubated for 3 days. Cell viability was measured by CTB assay. Briefly, 10 μ l of CTB reagent was added to each well, and cells were incubated for 2 h. Absorbance was measured at 570/590 nm using Perkin Elmer 2030 software.

Clonogenic assay

TNBC cells (300 4T1.2 cells or 300 E0771 cells per well) were plated in six-well plates. Twenty-four hours later, TP-0903 or vehicle was added to each well. Media were changed every 2 to 3 days for 9 days. Cells were then fixed and stained with crystal violet. Images were obtained using GelCount and counted using ImageJ software. The results were confirmed again by dissolving the crystal violet with 4% sodium deoxycholic acid and measuring absorbance at 595 nm using Perkin Elmer 2030 software.

Cell migration assay

IBC cells were treated with TP-0903 for 48 h and then subjected to a Boyden chamber migration assay, as previously described [25]. Briefly, SUM149 cells (2×10^5) or BCX010 cells (1×10^5) in serum-free medium were plated in the insert and then incubated at 37 °C in 5% CO₂ for 16 h. The inserts were then stained with 0.1% crystal violet for 10 min and analyzed using ImageJ software. To test the impact of AXL signaling in macrophages on the migration of human IBC cells, 100% CM from control macrophages and AXL-KO or inhibitor-treated

macrophages, collected after 48 h of culture, was used as an attractant in the bottom chamber of the inserts.

qRT-PCR

RNAs were extracted and purified using a PureLink RNA Mini Kit to analyze mRNA expression levels in cells and mouse tumor samples. cDNAs were synthesized from 1 µg of total RNA using amfiRivert cDNA Synthesis Platinum Master Mix. qRT-PCR was performed using specific primers listed in Supplementary Table 1. The reaction and data collection were performed using iTaq Universal SYBR Green Supermix and a CFX96 Real-Time PCR Detection System (Bio-Rad).

Western blot analysis

Cells were lysed using a buffer containing 50 mM Tris, pH 7.5, 150 mM NaCl, 1% NP40, 0.5% sodium deoxycholate acid, and 0.1% sodium dodecyl sulfate, supplemented with a protease and phosphatase inhibitor cocktail. Proteins from the lysates (30 µg per sample) were mixed with NuPAGE LDS Sample Buffer and heated at 95 °C for 5 min. The proteins were then separated by sodium dodecyl sulfate–polyacrylamide gel electrophoresis using 4–12% NuPAGE Bis–Tris gels and transferred onto an Immun-Blot polyvinylidene fluoride membrane. The proteins of interest were probed with specific primary antibodies followed by horseradish peroxidase–conjugated secondary antibodies. The blots were developed using Pierce ECL Western Blotting Substrate or SuperSignal West Dura Extended Duration Substrate and visualized on HyBlot CL autoradiography film using a Mini-Med 90 X-ray film processor.

ELISA

Protein levels of human CCL20, CCL26, EREG, CXCL9, and CXCL10 in lysates or CM from AXL-KO or control M2 macrophages were quantified using a DuoSet ELISA kit, following the manufacturer's instructions (R&D Systems). The absorbance of each sample was measured at 450 nm using a VICTOR X plate reader.

Mouse model studies

A suspension containing 4×10^6 SUM149 cells in 100 µl of 50% Matrigel was injected into the fourth inguinal mammary gland of 6- to 8-week-old female nu/nu mice. The mice were fed ad libitum with a regular diet and, after 3–4 weeks, when tumors reached approximately 75–100 mm³, mice were randomized into two groups and treated with a vehicle or TP-0903 (25 mg/kg) 5 days a week. Similarly, 1×10^5 BCX010 cells in 50% Matrigel were injected into female nu/nu mice and treated with TP-0903 (50 mg/kg) 5 days a week. For murine TNBC syngeneic models, 1×10^4 4T1.2 cells or 2.5×10^5 E0771

cells in 50% Matrigel were injected into the mammary fat pads of BALB/c and C57BL/6 mice, respectively. When tumors reached 75–100 mm³, mice were randomized into two groups and treated with a vehicle or TP-0903 (50 mg/kg) 5 days a week. Each group had 10–15 mice. Tumor volumes were measured twice a week, and tumor growth inhibition was calculated as previously described [26]. Mice were euthanized when tumor size reached the endpoint according to the MD Anderson Institutional Animal Care and Use Committee's regulations. Tumors were collected and subjected to further analysis.

For flow cytometric analysis, single cells were isolated from breast tumor tissues using a tumor dissociation kit according to the manufacturer's instructions (Miltenyi Biotec). The cells were filtered through 40 µm cell strainers and centrifuged at 2500 rpm for 10 min. Cell pellets were then resuspended with red blood cell lysis buffer and incubated for 1 min at 37 °C. After centrifuging at 2500 rpm for 5 min at 4 °C, the pellets were subjected to flow cytometric analysis.

For histological analysis, breast tumor tissues were fixed in 10% neutral buffered formalin, embedded in paraffin, and sectioned. For mRNA and protein quantification, small pieces of each tumor were lysed using the lysis buffer from the PureLink RNA Mini Kit for mRNA analysis or lysis buffer for Western blot analysis.

Flow cytometry

Single cell suspensions isolated from tumor tissues were stained with LIVE/DEAD Fixable Aqua Dead Cell Stain and primary antibodies in phosphate-buffered saline containing 2% FBS for 30 min on ice. These stained cells were analyzed using a Gallios flow cytometer (Beckman Coulter, Brea, CA), with appropriate single-color controls for compensation. Flow cytometric data were analyzed using FlowJo software.

Immunohistochemical (IHC) staining

Slides were dewaxed and rehydrated through a graded series of xylene and ethanol solutions. After rehydration, antigen retrieval was performed using microwave oven treatment with AR6 buffer. Once cooled down to room temperature (RT), slides were treated with 3% hydrogen peroxide at RT for 5 min to block endogenous peroxidase activity. Slides were then incubated with blocking solution for 30 min at RT, followed by overnight incubation with primary antibodies at 4 °C. Afterward, slides were incubated with secondary antibodies for 1 h at RT, followed by incubation with avidin–biotin complex reagent for 30 min at RT and then 3,3'-diaminobenzidine for 1–2 min at RT. The slides were counterstained with a hematoxylin solution for 10 s, mounted, and imaged using a Keyence

BZ-X 810 fluorescence microscope (Itasca, IL). Images were analyzed and quantified using ImageJ software.

RNA sequencing

Total RNAs were extracted from control and AXL-KO M2 macrophages and purified using a PureLink RNA Mini Kit. The mapping rates for all samples exceeded 85%, indicating high-quality libraries for sequencing. Three biological replicates of each macrophage group were sequenced using a NextSeq 500 high-output, 75-nt paired-end flow cell (Illumina, San Diego, CA). Transcript abundance was quantified using Salmon software. The reads were mapped to the reference genome GRCh38. Differential gene expression analysis was performed using DESeq2 software. Principal component analysis summarized the gene expression into two dimensions (PC1 and PC2).

Genes were considered differentially expressed if they had adjusted *P* values less than 0.05 and absolute log₂ fold change greater than 0.5. A volcano plot of $-\log_{10}(P \text{ value})$ versus log₂ fold change was generated. Using Enrichr software, Gene Ontology-based enrichment analysis was conducted for genes with adjusted *P* values less than 0.01 and log₂ fold change greater than 0.5 for upregulated genes or less than -0.5 for downregulated genes. All analyses were performed using the R computing language (version 4).

Analysis of AXL expression association with immune cell types in patients with IBC

The mRNA expression data from 137 clinical IBC samples, collected within the Inflammatory Breast Cancer International Consortium [27], were analyzed to assess the association between AXL expression and immune cell types deconvoluted using CIBERSORT.

Statistical analysis

All statistical analyses were performed using Prism software (version 9; GraphPad Software, Boston, MA). The number of migrating, growing, sphere-forming, or CD206⁺ cells was expressed as a percentage of the mean number of such cells in the vehicle-treated group or control group (“% of vehicle” or “% of control”). Data were analyzed using two-tailed Student’s *t*-test and analysis of variance with Dunnett’s correction for multiple comparisons. *P* values less than 0.05 were considered significant. Error bars in the graphs represent one standard deviation (SD).

Results

AXL inhibition reduces IBC tumor growth by suppressing the recruitment of TAMs

Our previous study showed that knockdown of AXL in SUM149 cells reduced their proliferation, migration, and invasion in vitro [25]. To further understand the role of

AXL in IBC progression, we inhibited AXL signaling in human IBC SUM149 and BCX010 cells using TP-0903, an AXL tyrosine kinase inhibitor. We tested the effect on cell migration and the cancer stem cell (CSC) population in vitro and tumor growth in vivo. As shown in Fig. 1A, TP-0903 treatment reduced the expression of phosphorylated AXL (pAXL) in SUM149 and BCX010 cells. Boyden chamber migration assay showed that TP-0903-treated SUM149 and BCX010 cells migrated less than vehicle-treated cells (Fig. 1B). CSC enrichment has been reported to contribute to IBC aggressiveness [28]. We examined the role of AXL in CSC regulation using a surrogate mammosphere formation assay, which showed that TP-0903 treatment reduced primary and secondary mammosphere formation of SUM149 and BCX010 IBC cells (Fig. 1C). These results suggest that AXL inhibition reduces migration and the CSC population of IBC cells. Moreover, treatment with TP-0903 at 25 mg/kg in a SUM149 xenograft model and 50 mg/kg in a BCX010 xenograft model significantly reduced tumor growth (Fig. 1D) without notable body weight loss (Supplementary Fig. 1A), indicating that inhibition of AXL signaling suppresses IBC tumor growth.

Previous studies demonstrated that a high level of CD206⁺ macrophage infiltration is one of the hallmarks of IBC [11, 29]. Further, high CD206 expression in tumor macrophages often correlates with a pro-tumoral, immunosuppressive phenotype. Thus, we used flow cytometry to analyze CD206⁺ macrophage populations in tumor tissues from vehicle- and TP-0903-treated SUM149 xenografts (Supplementary Fig. 1B). As shown in Fig. 2A and Supplementary Fig. 1C, TP-0903-treated tissues had less infiltration of CD206⁺ macrophages (CD45⁺CD11b⁺Ly6C⁻Ly6G⁻F4/80⁺CD206⁺ cells) than did vehicle-treated tissues. IHC staining further confirmed lower CD206 expression in TP-0903-treated tumor tissues than in vehicle-treated tissues (Fig. 2B). These results suggest that AXL signaling inhibition reduces CD206⁺ macrophage infiltration.

To further test the effects of AXL inhibition on tumor growth and the TME in aggressive breast cancer, we extended our investigations to murine TNBC 4T1.2 and E0771 immunocompetent syngeneic mouse models due to the non-availability of an IBC immunocompetent syngeneic mouse model. We first confirmed that TP-0903 inactivated the AXL pathway (Supplementary Fig. 2A) and reduced these murine cells’ colony formation and migration capabilities in vitro (Supplementary Fig. 2B, C). Next, we examined the effect of TP-0903 on 4T1.2 and E0771 tumor growth and immune responses using flow cytometric analysis. TP-0903 treatment at 50 mg/kg significantly reduced tumor growth and the numbers of macrophages in 4T1.2 (CD206⁺ cells) and E0771

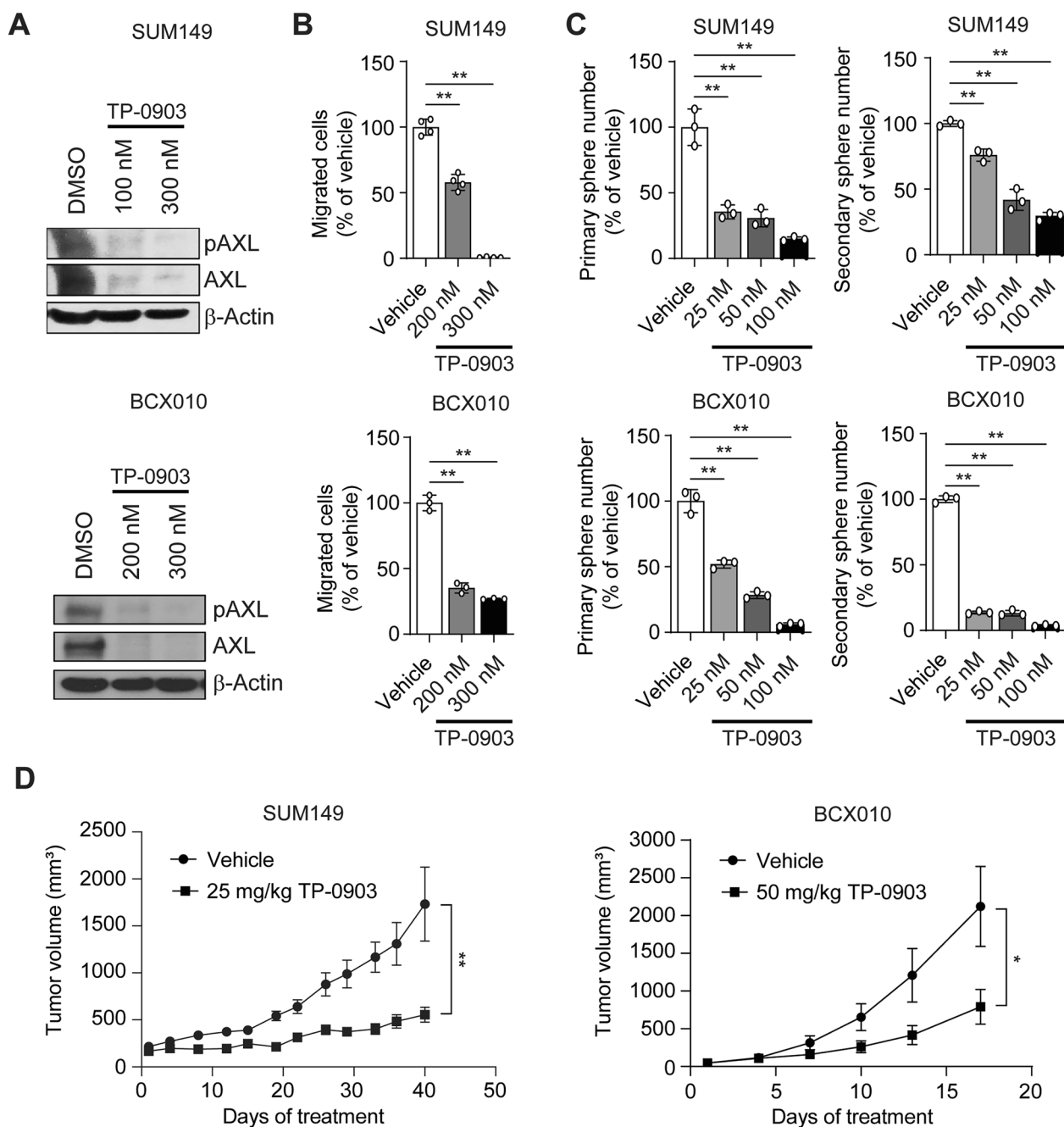


Fig. 1 TP-0903 treatment inhibits AXL signaling and reduces IBC cell migration and mammosphere formation in vitro and tumor growth in vivo. **A** TP-0903 reduced phospho-AXL and total AXL protein expression in SUM149 and BCX010 IBC cells as determined using Western blotting. **B** TP-0903 reduced SUM149 and BCX010 cell migration as tested using transwell migration assay. The mean number of migrated cells was determined for the 4 vehicle replicates in SUM149 and 3 vehicle replicates in BCX010. For each sample (12 each for SUM149 and 9 each for BCX010), the number of migrated cells, relative to the mean in the vehicle group, was plotted as a percentage (“% of vehicle”). **C** TP-0903 reduced primary and secondary mammosphere formation of SUM149 and BCX010 cells as determined using a surrogate mammosphere formation assay. **D** Tumor growth curves for vehicle- and TP-0903-treated groups in human IBC xenograft mouse models. TP-0903 decreased SUM149 and BCX010 tumor volumes in mice. SUM149 xenograft model: $n = 12$ mice; BCX010 xenograft model: $n = 14$ mice. Data were summarized as means \pm SD in **B** and **C** and means \pm SEM in **D**. One-way analysis of variance followed by Dunnett’s multiple comparison test (**B** and **C**) or 2-tailed Student *t* test (**D**) was used to calculate *P* values. * $P < 0.05$; ** $P < 0.01$

(CD45⁺CD11b⁺F4/80⁺Ly6C⁻Ly6G⁻ cells) murine mammary tumors (Fig. 2C, D, and Supplementary Fig. 2D, E). IHC staining showed lower CD206 expression in TP-0903-treated tissues than in vehicle-treated tissues in the E0771 mouse model (Fig. 2E). Furthermore, TP-0903 treatment decreased the population of Tregs (CD45⁺CD3⁺CD4⁺CD25⁺FOXP3⁺ cells) in both 4T1.2 and E0771 tumor tissues (Fig. 2F and Supplementary Fig. 3). Taken together, these results suggest that suppressing the AXL pathway inhibits the growth of human IBC and murine TNBC tumors while also reducing the infiltration of CD206⁺ macrophages and Tregs into tumors.

AXL signaling contributes to the polarization of immunosuppressive M2 macrophages

Given that TAMs drive the aggressiveness of IBC, we next asked whether AXL regulates the polarization of M2 macrophages. To answer this question, we knocked out AXL in human THP-1 monocytes using the CRISPR/Cas9 system, induced their differentiation into M2 macrophages with IL-4 and IL-13 cytokines, and confirmed AXL depletion in the resulting M2 macrophages using Western blotting (Fig. 3A). AXL KO did not impact the viability of THP-1-polarized M2 macrophages (Supplementary Fig. 4A, B). We then conducted qRT-PCR to assess the effect of AXL suppression on the expression of M2 macrophage markers and secreted chemokines. Our analysis revealed that M2 macrophages polarized from AXL-depleted THP-1 cells exhibited reduced expression of CD163 and CD206 (Fig. 3B), which are traditional markers of M2 macrophages, and also reduced expression of the cytokines CCL17 and CCL18 (Fig. 3B), both of which are typically secreted in high amounts by M2 macrophages [30, 31]. Indeed, flow cytometry analysis showed that AXL-depleted monocytes generated fewer CD206⁺ macrophages when polarized with IL-4 and IL-13 than control monocytes did (Fig. 3C and Supplementary Fig. 4C).

In addition to the genomic KO approach, we used TP-0903 to inactivate AXL signaling in THP-1 monocytes and examined the effect on M2 macrophage polarization. Specifically, we treated M0 macrophages with TP-0903 while polarizing them into M2 macrophages and examined the impact on M2 macrophage markers and secreted chemokines. Treatment with TP-0903 decreased AXL mRNA and protein levels in THP-1-derived M2 macrophages (Fig. 3D), confirming the inactivation of AXL signaling. TP-0903 treatment also reduced expression of M2 macrophage markers *CD163* and *CD206*, along with M2-secreted cytokines *CCL17* and *CCL18* (Fig. 3E). Furthermore, flow cytometric and Western blot analyses showed that TP-0903 treatment reduced both the CD206⁺ population and CD206 protein level in these M2 macrophages (Fig. 3F and Supplementary Fig. 4D). In summary, these results suggest that AXL signaling regulates the polarization of M2 macrophages.

M2 macrophage-derived AXL signaling promotes the growth and migration of IBC cells

Given that TP-0903 treatment reduced IBC growth and CD206⁺ macrophage infiltration (Figs. 1, 2) and that AXL signaling regulated the polarization of M2 macrophages (Fig. 3), we hypothesized that the AXL signaling pathway modulates the biological impact of M2 macrophages on IBC cells. To test this hypothesis, we examined how inhibiting AXL in M2 macrophages affects the growth and motility of IBC cells. We collected CM from TP-0903-treated or AXL-KO M2 macrophages and the respective controls after 48 h of culture and co-cultured 100% CM with IBC cells for growth assays and migration assays. As shown in Fig. 4A, IBC cells grew slower when co-cultured with CM from M2 macrophages treated with TP-0903 than when co-cultured with CM from vehicle-treated M2 macrophages, as determined using CTB assay. Additionally, the CM from TP-0903-treated M2 macrophages induced less migration of SUM149

(See figure on next page.)

Fig. 2 TP-0903 treatment suppresses the population of CD206⁺ macrophages in human IBC xenograft and murine TNBC syngeneic models. **A** Tumors from a SUM149 xenograft mouse model treated with vehicle or TP-0903 for 7 days were dissociated to obtain a single-cell suspension and stained with antibodies. Flow cytometric analysis showed a decreased CD206⁺ macrophage population (CD45⁺CD11b⁺Ly6C⁻Ly6G⁻F4/80⁺CD206⁺ cells) after TP-0903 treatment. **B** IHC staining of CD206 on slides from the above tumor sections. TP-0903 decreased the population of CD206⁺ cells in SUM149 tumor tissues. Left panel: representative IHC staining images. Scale bar = 200 μm. Right panel: quantification of CD206 expression by ImageJ. **C** Tumor growth curves for the vehicle- and TP-0903-treated groups in murine TNBC syngeneic mouse models. TP-0903 suppressed the growth of 4T1.2 and E0771 mammary tumors in vivo. **D** TP-0903 treatment reduced CD206⁺ macrophages in murine mammary tumors from the 4T1.2 mouse model. **E** IHC staining for CD206 showed reduced CD206⁺ cells in TP-0903-treated tumor tissues from E0771 mice. Left panel: representative IHC staining images. Scale bar = 200 μm. Right panel: quantification of CD206 expression. **F** Flow cytometric analysis showed a decrease in Tregs (CD45⁺CD3⁺CD4⁺CD25⁺FOXP3⁺ cells) in TP-0903-treated 4T1.2 and E0771 mice. 4T1.2 syngeneic model: *n* = 10 mice; E0771 syngeneic model: *n* = 15 mice. Data were summarized as means ± SD in **A**, **B**, and **D** to **F** and means ± SEM in **C**. A 2-tailed Student *t* test was used to calculate *P* values. **P* < 0.05; ***P* < 0.01

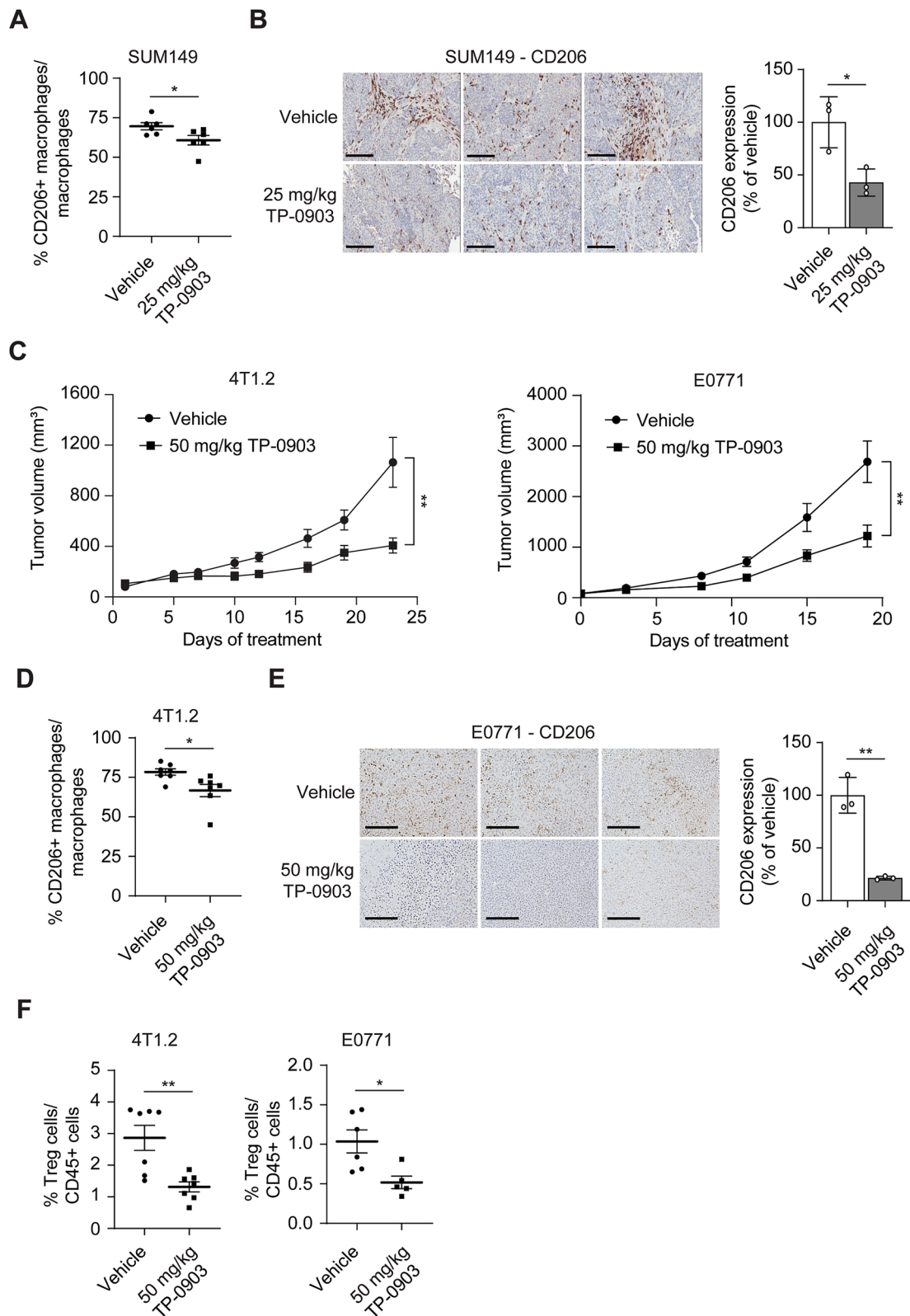


Fig. 2 (See legend on previous page.)

and BCX010 cells than the CM from vehicle-treated M2 macrophages did (Fig. 4B). Similarly, IBC cells exhibited slower growth and less migration when co-cultured with CM from M2 macrophages polarized from AXL-KO THP-1 cells than when co-cultured with CM from M2 macrophages polarized from control THP-1 cells (Fig. 4C, D). In summary, these results demonstrate that AXL signaling regulates the polarization of immunosuppressive M2 macrophages, thereby promoting the growth and migration of IBC cells.

AXL signaling contributes to the polarization of immunosuppressive M2 macrophages via STAT6

Next, we investigated the molecular mechanism by which AXL signaling regulates the polarization of M2 macrophages. It has been reported that transcription factor STAT6 plays a key role in modulating the polarization and functions of M2 macrophages, and IL-4 and IL-13 activate the JAK2/STAT6 signaling pathway, promoting the transcription of STAT6-responsive genes [32–34]. Therefore, we hypothesized that AXL signaling regulates the polarization and functions of M2 macrophages via STAT6.

To test this hypothesis, we treated M2 macrophages polarized from THP-1 cells with TP-0903 and observed a reduction in both the phosphorylation and total levels of STAT6 (Fig. 5A). Similar results were obtained in M2 macrophages polarized from AXL-KO THP-1 cells compared to M2 macrophages polarized from control cells (Fig. 5B). These results demonstrate that the AXL pathway regulates STAT6 signaling in M2 macrophages. Additionally, we knocked down STAT6 in THP-1 cells (Fig. 5C). We found a reduction in the CD163⁺CD206⁺ macrophage population, as determined via flow cytometry (Fig. 5D), and a decrease in the expression of M2 markers *CD163* and *CD206* (Fig. 5E).

To further confirm that AXL regulates M2 macrophage polarization and functions via STAT6, we overexpressed STAT6 in M2 macrophages polarized from both control

and AXL-KO THP-1 cells (Fig. 5F). This overexpression enhanced the expression of the M2 macrophage markers *CD163* and *CD206*, as well as *CCL17* and *CCL18*, in M2 macrophages polarized from AXL-KO THP-1 cells (Fig. 5G). Moreover, CM from STAT6-overexpressing M2 macrophages mitigated the inhibitory effect of AXL depletion on the migration of SUM149 cells (Fig. 5H). These results demonstrate that AXL signaling regulates polarization and mediates the impact of M2 macrophages on IBC cells via STAT6, highlighting a crucial regulatory axis in the TME.

M2 macrophage-derived AXL signaling generates an immunosuppressive TME

Next, to further understand the impact of M2 macrophage-derived AXL signaling on the IBC TME and the underlying molecular mechanism, we performed RNA sequencing analysis on M2 macrophages polarized from AXL-KO and control THP-1 cells. Principal component analysis showed a clear separation of control and AXL-KO samples (Supplementary Fig. 5A), indicating that the difference in the experimental conditions (control vs. AXL KO) accounted for the observed differences in gene expression (Supplementary Fig. 5B). We validated significant downregulation of genes involved in M2 polarization, such as *CD209*, *IL13RA1*, and *IL2RG*, in AXL-KO THP-1-derived M2 macrophages (Fig. 6A). *CD209*, also known as dendritic cell-specific ICAM-3-grabbing non-integrin, is highly expressed in M2 macrophages [35]. *IL-13RA* ($\alpha 1$) and *IL-2RG* (γC) are subunits of receptors that bind to IL-4 and IL-13, cytokines that drive M2 macrophage polarization [36]. These results further confirm AXL's role in regulating the polarization of immunosuppressive M2 macrophages.

We further analyzed the pathways in M2 macrophages regulated by AXL. Gene Ontology-based enrichment analysis demonstrated that depleting AXL in M2 macrophages suppressed pathways related to cytokine production and cellular response to cytokine stimulus,

(See figure on next page.)

Fig. 3 AXL inhibition suppresses the polarization of immunosuppressive M2 macrophages. **A** AXL was knocked out in human THP-1 monocytes using the CRISPR/Cas9 system. These cells and control cells were subsequently induced into M2 macrophages, and AXL depletion was confirmed in AXL-KO M2 macrophages using Western blotting. M2 macrophages polarized from AXL-KO THP-1 cells had lower expression of AXL than M2 macrophages polarized from control cells. **B** The expression of M2 macrophage markers and secreted cytokines was measured by qRT-PCR. AXL KO reduced the expression of *CD163*, *CD206*, *CCL17*, and *CCL18* in M2 macrophages. **C** Flow cytometric analysis was conducted to compare the CD206⁺ macrophage population polarized from AXL-KO versus control THP-1 cells. AXL KO reduced the population of CD206⁺ macrophages polarized from THP-1 cells. **D** Treatment with TP-0903 inhibited the expression of AXL mRNA (left panel) and protein (right panel) in THP-1-derived M2 macrophages as determined using qRT-PCR and Western blotting, respectively. **E** TP-0903-treated M2 macrophages showed reduced mRNA level of *CD163*, *CD206*, *CCL17*, and *CCL18* compared to vehicle-treated M2 macrophages. **F** Flow cytometry and Western blotting showed that TP-0903 reduced the population of CD206⁺ cells (left panel) and CD206 protein expression (right panel) in THP-1-derived M2 macrophages. All experiments were repeated at least three times. Data were summarized as means \pm SD. A 2-tailed Student t test (**B** and 1-way analysis of variance followed by Dunnett's multiple comparison test (**D–F**) were used to calculate *P* values. **P* < 0.01

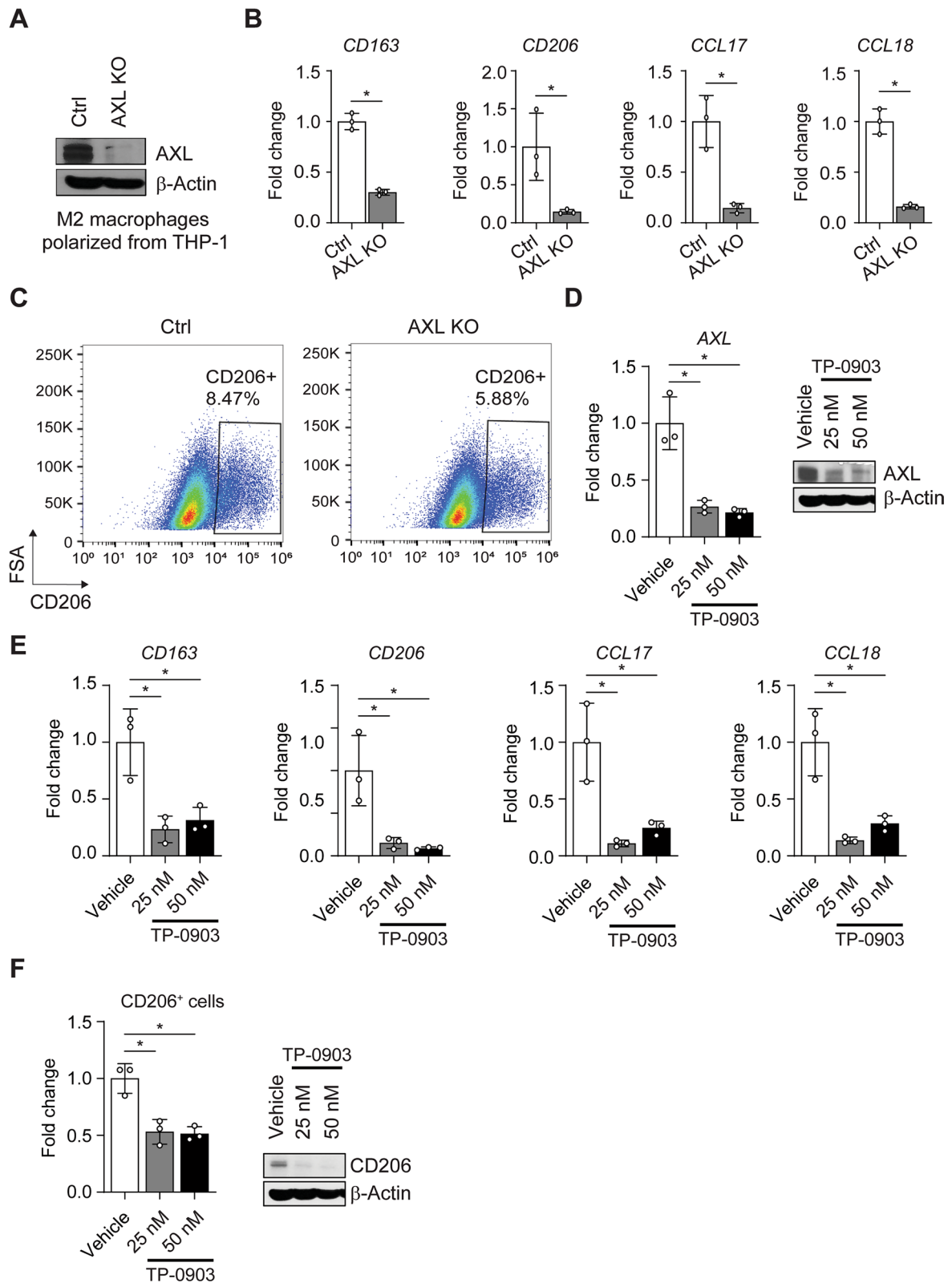


Fig. 3 (See legend on previous page.)

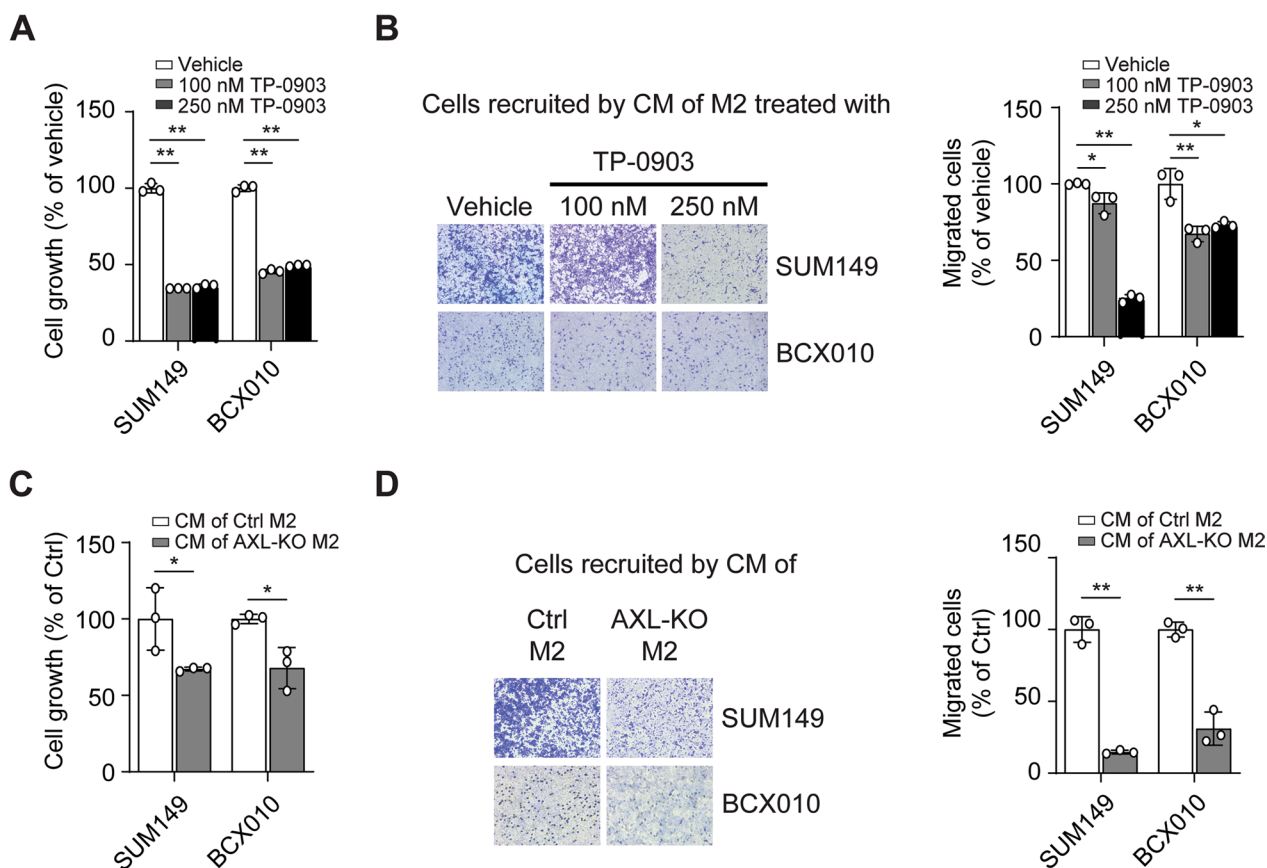


Fig. 4 AXL depletion reduces the impact of M2 macrophages on IBC cell growth and migration. **A** SUM149 and BCX010 cells were co-cultured with 100% CM collected after culturing vehicle- or TP-0903–treated M2 macrophages for 48 h, and cell numbers after 3 days were measured by CTB assay. CM from TP-0903–treated M2 macrophages reduced the growth of SUM149 and BCX010 IBC cells. **B** The migration of human IBC cells induced by 100% CM from TP-0903– or vehicle-treated M2 macrophages after 48 h of culture was examined using transwell migration assay. CM from TP-0903–treated M2 macrophages inhibited the migration of SUM149 and BCX010 cells (**C**). **D** 100% CM from AXL-KO M2 macrophages after 48 h of culture reduced the growth **C** and migration **D** of SUM149 and BCX010 cells. All experiments were repeated at least three times. Data were summarized as means ± SD. One-way analysis of variance followed by Dunnett’s multiple comparison test (**A** and **B**) and 2-tailed Student t test (**C** and **D**) were used to calculate *P* values. **P* < 0.05; ***P* < 0.01

(See figure on next page.)

Fig. 5 AXL suppression inhibits the polarization of immunosuppressive M2 macrophages via STAT6. **A** Treatment with TP-0903 reduced AXL, phospho-STAT6, and STAT6 protein expression as determined by Western blotting. **B** M2 macrophages polarized from AXL-KO THP-1 cells had lower phospho-AXL, AXL, phospho-STAT6, and STAT6 protein expression than those polarized from control THP-1 cells, as determined using Western blotting. **C–E** STAT6 was knocked down in THP-1 cells using siRNAs, and then THP-1 cells were induced to M2 macrophages. Knockdown of STAT6 in THP-1–polarized M2 macrophages **C** decreased the CD163⁺CD206⁺ macrophage population as determined by flow cytometry **D** and decreased the expression of the *CD163* and *CD206* genes as determined using qRT-PCR **E**. **F** STAT6 was overexpressed in M2 macrophages polarized from AXL-KO THP-1 cells as tested using qRT-PCR. **G** STAT6 overexpression mitigated the inhibitory effect of AXL KO on the expression of M2 macrophage markers and cytokines, including *CD163*, *CD206*, *CCL17*, and *CCL18*. **H** The CM from control, AXL-KO, and AXL-KO + STAT6–overexpressing M2 macrophages and fresh media were used as attractants plated in the bottom chamber of transwells to test the migration of SUM149 cells. Migration of SUM149 cells was greater with CM from AXL-KO + STAT6–overexpressing M2 macrophages than with CM from AXL-KO M2 macrophages. All experiments were repeated at least three times. Data were summarized as means ± SD. One-way analysis of variance followed by Dunnett’s multiple comparison test was used to calculate *P* values. **P* < 0.05; ***P* < 0.01

but it increased the regulation of response to type I interferon–mediated signaling (Supplementary Fig. 5C). We then performed qRT-PCR to validate the effect

of AXL depletion on the expression of downstream candidates in M2 macrophages. We confirmed reduced expression of immunosuppressive chemokines, such as

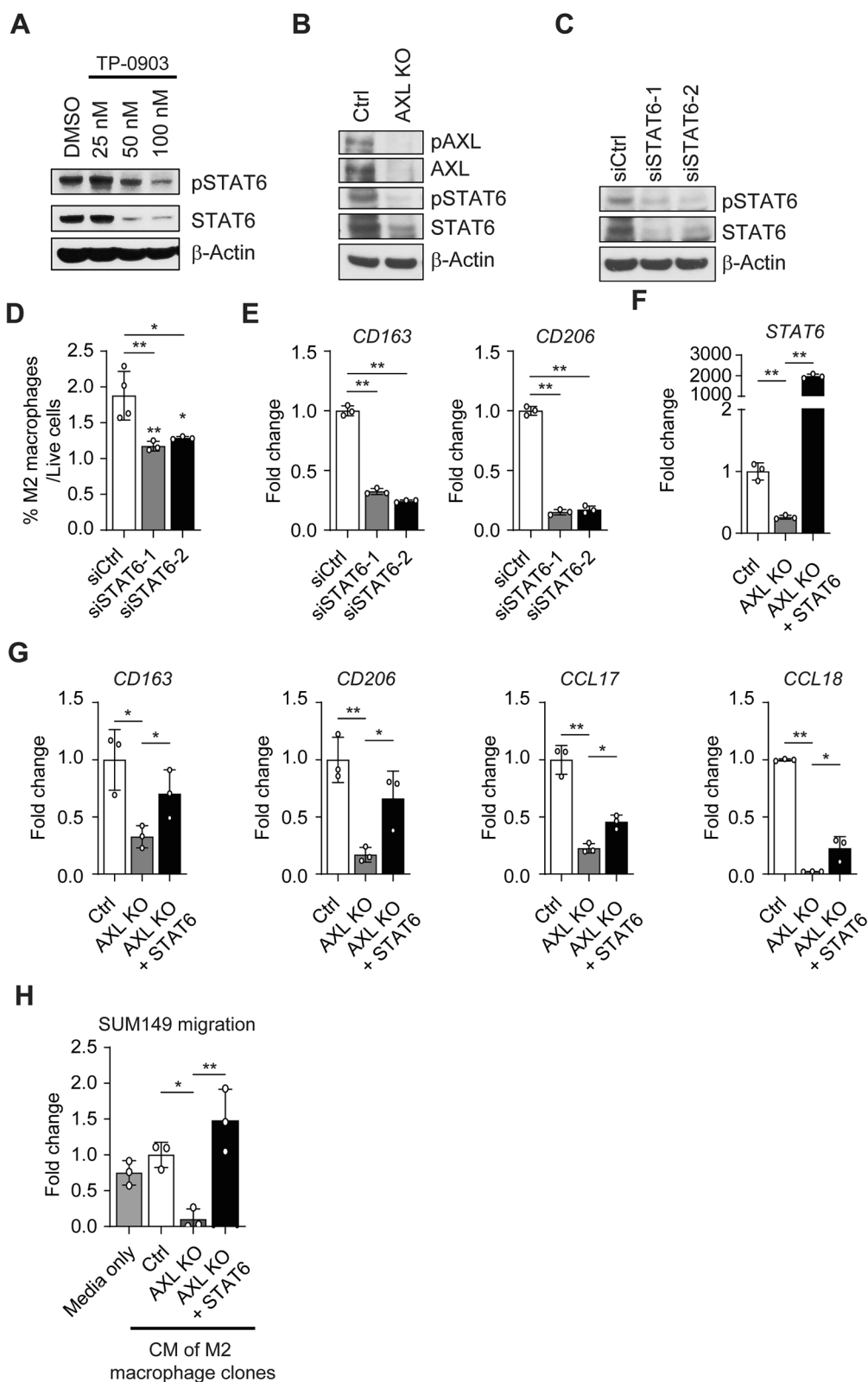


Fig. 5 (See legend on previous page.)

CCL20 [37], *CCL26* [38], *EREG* [39], and *IL1B* [40], in AXL-KO-derived M2 macrophages (Fig. 6B). Moreover, AXL depletion in M2 macrophages also reduced the expression of molecules involved in modulating an immunosuppressive TME, including *APOC2* [41], *MFNG* [42], *TIMP2* [43], and *GPR68* [44] (Supplementary Fig. 6A). In contrast, AXL depletion increased the mRNA expression of immunoactive chemokines involved in the interferon γ -mediated signaling pathway, such as *IFNG*, *CXCL10*, and *GBP2* [45–50] (Fig. 6C). Inactivating AXL signaling in THP-1-derived M2 macrophages with TP-0903 had similar effects on the expression of cytokines and modulators involved in creating an immunosuppressive TME (Supplementary Fig. 6B–E). We also validated protein level changes for cytokines, including decreased levels of CCL20, CCL26, and EREG (Fig. 6D) and increased levels of CXCL9 and CXCL10 (Fig. 6E), in M2 macrophages polarized from AXL-KO THP-1 cells using ELISA.

Cytokines play a crucial role in mediating cancer metastasis promoted by M2 macrophages [51]. For example, CCL20, secreted by TAMs, has been shown to stimulate the growth and migration of endometriotic stromal cells [52] and pancreatic cancer cells [53]. CCL26 promotes the invasion of colorectal cancer by inducing TAM infiltration [54]. Additionally, EREG has been implicated in enhancing the migration and invasion of salivary adenoid cystic carcinoma [55] and oral squamous cell carcinoma [56]. Therefore, we hypothesized that the macrophage-derived AXL pathway regulates the migration of IBC cells via immunosuppressive cytokines, including CCL20, CCL26, and EREG. To test this hypothesis, we examined the migration of IBC cells induced by CM from AXL-KO M2 macrophages with or without the addition of recombinant CCL20, CCL26, or EREG proteins. Indeed, recombinant CCL20, CCL26, or EREG protein mitigated the reduced migration of SUM149 and BCX010 cells induced by AXL-KO M2

macrophages (Fig. 6F). Furthermore, to examine whether AXL regulates the secretion of CCL20, CCL26, or EREG via the STAT6 pathway, we overexpressed STAT6 in M2 macrophages polarized from AXL-KO THP-1 cells and examined the secretion of these cytokines. The results indicated that STAT6 overexpression mitigated the inhibitory effect of AXL depletion on the expression of these cytokines (Fig. 6G).

In summary, our data suggest that AXL signaling in M2 macrophages regulates the expression of cytokines and molecules involved in creating an immunosuppressive TME via the STAT6 signaling pathway and this regulation induces the migration of IBC cells.

AXL signaling correlates with an immunosuppressive TME in IBC patient samples

To explore the role of AXL expression in tumor-infiltrating immune cells, we analyzed AXL mRNA expression in tumor tissues from 137 IBC patients collected within the Inflammatory Breast Cancer International Consortium [57] using CIBERSORT deconvolution. We found that patients with high AXL expression had significantly more M2 macrophages (mean, 9.85 [range, 0.78–22.36] vs. 7.93 [range, 0–24.62]; $P=0.0411$; Fig. 7A) and resting memory CD4⁺ T cells (mean, 3.83 [range, 0–18.06] vs. 2.43 [range, 0–10.26]; $P=0.0312$; Fig. 7B) compared to those with low AXL expression. M2 macrophages are known to suppress immune activation and exert immunosuppressive functions, which are associated with poorer overall survival [11, 58, 59]. Resting memory CD4⁺ T cells are functionally and metabolically quiescent cells [60] that positively correlate with high-risk immune groups and poor prognosis [61–65].

Additionally, IBC patients with high AXL expression had fewer activated myeloid dendritic cells (mean, 0.23 [range, 0–2.96] vs. 0.56 [range, 0–5.70]; $P=0.0263$; Fig. 7C) and follicular helper T cells (mean, 2.70 [range,

(See figure on next page.)

Fig. 6 AXL regulates the expression of cytokines via STAT6 in M2 macrophages. **A–C** mRNA was collected from M2 macrophages polarized from AXL-KO THP-1 and control cells, and the expression of M2 macrophage markers or cytokines/chemokines was examined using qRT-PCR. AXL KO in M2 macrophages derived from THP-1 cells reduced the mRNA expression of *CD209*, *IL13RA*, and *IL2RG* **A**. AXL KO in M2 macrophages derived from THP-1 cells reduced the expression of the immunosuppressive cytokines/chemokines *CCL20*, *CCL26*, *EREG*, and *IL1B* **B**. AXL KO in M2 macrophages derived from THP-1 cells increased the expression of cytokines/chemokines involved in the interferon γ -mediated signaling pathway, such as *IFNG*, *CXCL10*, and *GBP2*, at the gene level **C**. **D** and **E** CM from and lysates of M2 macrophages polarized from AXL-KO THP-1 cells had decreased expression of CCL20, CCL26, and EREG protein **D** but increased expression of CXCL9 and CXCL10 protein **E** as determined using ELISA. **F** The migration of human IBC cells was assessed using a transwell migration assay, with CM collected from control and AXL-KO M2 macrophages with or without the addition of recombinant CCL20, CCL26, and EREG protein, serving as attractants. CCL20, CCL26, and EREG mitigated the inhibitory effect of AXL-KO M2 macrophages on SUM149 and BCX010 cell migration. **G** qRT-PCR was conducted to measure the mRNA expression level of *CCL20*, *CCL26*, and *EREG* in control, AXL-KO, and AXL-KO + STAT6-overexpressing M2 macrophages. Overexpression of STAT6 mitigated the suppressive effect of AXL KO in M2 macrophages on the expression of *CCL20*, *CCL26*, and *EREG* genes. All experiments were repeated at least three times. Data were summarized as means \pm SD. Two-tailed Student *t* test (**A–E**) and 1-way analysis of variance followed by Dunnett's multiple comparison test (**F** and **G**) were used to calculate *P* values. * $P < 0.05$; ** $P < 0.01$; *** $P < 0.001$

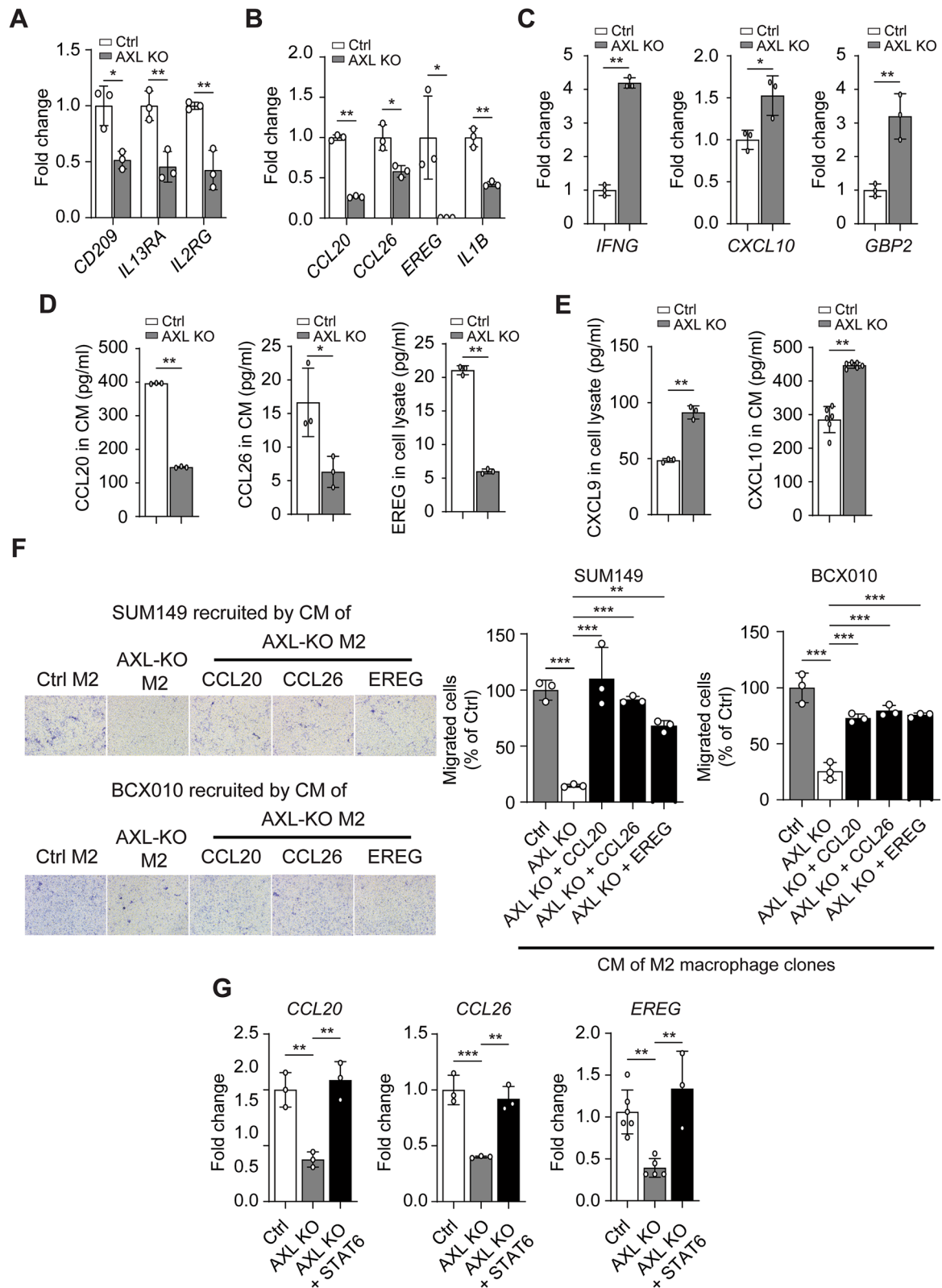


Fig. 6 (See legend on previous page.)

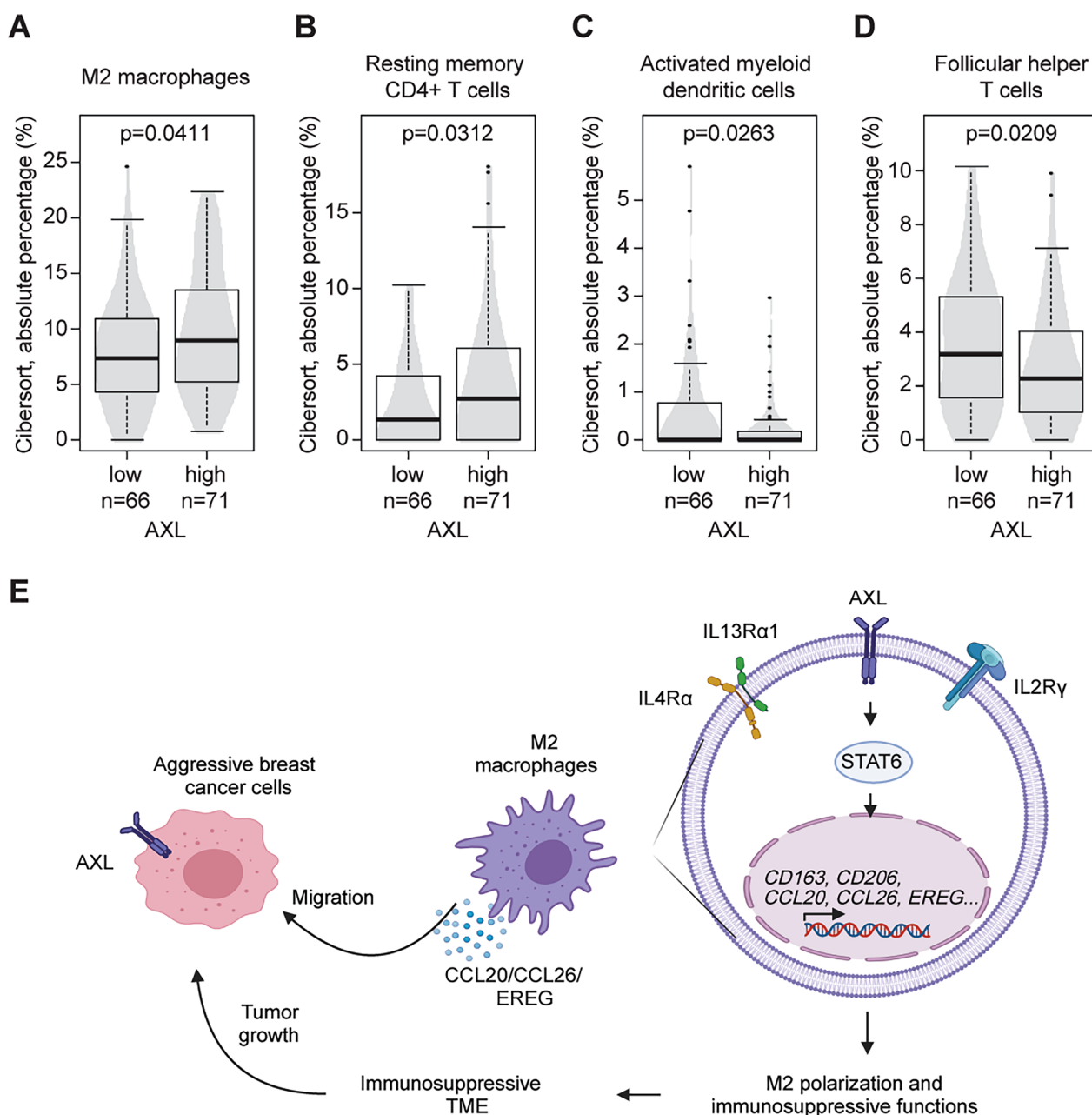


Fig. 7 AXL expression correlates with an immunosuppressive TME of IBC. **A–D** Violin plots showed the absolute percentages of different immune cell subsets as defined by CIBERSORT according to high versus low AXL expression in IBC samples from the Inflammatory Breast Cancer International Consortium: M2 macrophages **A**, resting memory CD4⁺ T cells **B**, activated myeloid dendritic cells **C**, and follicular helper T cells **D**. A 2-tailed Student t test was used to calculate P values. **E** Proposed mechanistic model of AXL in the IBC TME. AXL regulated M2 macrophage polarization and the expression of immunosuppressive molecules and STAT6-modulated cytokines, which induced IBC’s aggressiveness

0–9.88] vs. 3.64 [range, 0–10.13]; $P=0.0209$; Fig. 7D) than those with low AXL expression. Both dendritic cells [66, 67] and CD4⁺ follicular helper T cells [68] can mediate anti-tumor immunity and are positively associated with better prognosis and response to immunotherapy in different solid tumors.

Taken together, the higher levels of M2 macrophages and resting memory CD4⁺ T cells and lower levels of activated myeloid dendritic cells and follicular helper T cells in patient samples with high AXL expression may reflect an immunosuppressive TME regulated by the AXL pathway in patients with IBC.

Discussion

In this study, we demonstrated that AXL signaling promotes IBC growth by regulating both tumor cells and immunosuppressive CD206⁺ macrophages, as illustrated in Fig. 7E. AXL regulates several key processes in IBC, including proliferation, migration, invasion, tumor growth, and notably, the polarization of monocytes into M2 macrophages and the secretion of chemokines such as CCL20, CCL26, and EREG via STAT6 signaling, contributing to an immunosuppressive TME in IBC.

IBC tumors exhibit a higher infiltration of TAMs compared to other types of breast cancer [11]. Interactions between IBC cells and macrophages promote IBC's aggressiveness, and secreted factors from IBC tumors induce macrophage differentiation more than secreted factors from non-IBC tumors do [11]. These findings underscore the critical role of macrophages in IBC progression and the urgent need for effective therapies targeting TAMs. We showed that depleting AXL protein or inactivating its signaling inhibited the polarization of monocytes to M2 macrophages, thereby inhibiting IBC cell growth and migration promoted by M2 macrophages. To our knowledge, this study is the first to identify AXL within TAMs as an effective therapeutic target for IBC.

CD206 has been used as a prominent marker for "M2-like" macrophages with immunosuppressive, tumor-promoting functions. Previous studies have demonstrated that CD206^{high} macrophages are attracted from the stroma into the epithelial layer by cancer cell-secreted CCL2, driving early dissemination and metastasis via secreted Wnt-1 [69]. In IBC, tumor cells have been shown to attract monocytes and differentiate them into tumor-promoting, immune-suppressing M2-like macrophages with elevated expression of CD206, CD163, and CD209 [11]. Additionally, mesenchymal stem cell-secreted IL-6 induces the polarization and pro-tumor functions of CD206⁺ macrophages in IBC mouse models [10]. Our findings further highlight the tumor-promoting role of CD206⁺ macrophages by demonstrating the contribution of AXL within these cells to IBC progression.

However, it is essential to recognize that macrophages exist along a dynamic spectrum of activation states and molecular diversity, with different subsets contributing to tumor progression through different mechanisms. For instance, a single-cell RNA sequencing (scRNA-seq) analysis revealed that tissue-resident FOLR2⁺ macrophages positively correlated with T cell infiltration and improved prognosis in breast cancer patients [70]. Similarly, Ray et al. recently demonstrated, using a novel conditional CD206 knock-in mouse, that TAMs expressing CD206 play a critical role in early T cell

recruitment [71]. Intriguingly, their study also identified a CD206^{Replete} gene signature that correlated with CD8 T cell, cDC1, and NK signatures and was associated with better survival. These findings emphasize the complexity of TAM biology and suggest that CD206⁺ macrophages may also exert context-dependent pro- and anti-tumor effects.

Additionally, recent studies have highlighted the unique expression of AXL in distinct macrophage subsets. A pan-cancer analysis of single myeloid cells from 210 patients across 15 human cancer types identified AXL as one of the key mutated genes in the inflammatory response pathway, primarily expressed in C1QC⁺ TAMs [72]. Another scRNA-seq study demonstrated exclusive expression of AXL in MMP9⁺ macrophages [73]. These findings suggest that AXL may regulate diverse macrophage subsets with various roles in the TME. Understanding the impact of targeting AXL on these subsets is essential for developing effective therapeutic strategies.

We elucidated the molecular mechanism by which AXL regulates the polarization of immunosuppressive M2 macrophages. Targeting AXL reduces the expression of IL-2RG and IL-13RA in M2 macrophages, key components of IL-4 and IL-13 receptor complexes [36, 74]. These complexes activate JAKs and subsequently STAT6, promoting M2 macrophage polarization. Our findings suggest that AXL promotes M2 polarization via regulation of IL-4/IL-13 receptors and STAT6 signaling.

Our study also highlights how AXL affects the broader immune cell components in the IBC TME. High AXL expression is associated with larger populations of M2 macrophages [11, 58, 59] and resting memory CD4⁺ T cells [61–65], which positively correlate with high-risk immune groups, but smaller populations of immune cells that enhance immune responses, such as activated myeloid dendritic cells [66, 67] and follicular helper T cells [68]. These findings suggest that high AXL expression is correlated with an immunosuppressive TME in patients with IBC.

We further identified key molecules modulated by AXL in M2 macrophages, including CD209, APOC2, MFNG, TIMP2, and GPR68, which are implicated in creating an immunosuppressive TME. For example, high infiltration of CD209⁺ TAMs is associated with Treg expansion [75] and CD8⁺ T cell tolerance [76], while APOC2 [77], MFNG [78], TIMP2 [79], and GPR68 [80] are linked with TAM regulation, T cell exhaustion, and immune evasion. We found that targeting AXL in M2 macrophages reduced the expression of these molecules, supporting its role in sustaining an immunosuppressive TME.

In addition, AXL inhibition alters cytokine profiles in the IBC TME, reducing immunosuppressive cytokines (e.g., IL1B, CCL20, CCL26, and EREG) and increasing T cell-activating cytokines (e.g., IFNG, CXCL9, CXCL10, and GBP2) [81–83]. Notably, we recently showed that EREG, a ligand for EGFR, promoted an immunosuppressive TME in IBC [27]. EREG is also expressed in macrophages and promotes cancer progression via EGFR activation [84]. Our findings suggest that targeting AXL may inhibit EGFR signaling in M2 macrophages, warranting further investigation into the interplay between AXL and EGFR in modulating the IBC TME.

Although our study focused on AXL in macrophages, tumor-derived AXL signaling also modulates the TME. Activated AXL signaling in oral squamous cell carcinoma induces TAM polarization toward M2 phenotype with pro-tumor functions via the PI3K/Akt/NF- κ B pathway [22]. Lung cancer cells can activate AXL signaling in TAMs through secreted IL-11 and induce the recruitment of TAMs in a mouse model [85]. These interactions highlight the complex crosstalk between tumor cells and TAMs and emphasize the need for future studies to dissect the role of the tumor-derived AXL pathway in modulating the IBC TME.

The limitations of our study include the lack of syngeneic IBC mouse models, which prevented us from investigating the effect of macrophage-derived AXL signaling on other immune cells, such as T cells and Tregs. However, the consistent findings in syngeneic TNBC mouse models support AXL's role in recruiting immunosuppressive Tregs. Further studies utilizing conditional AXL-KO or humanized IBC mouse models will be essential to reveal these mechanisms underlying the effects of macrophage-derived AXL signaling on other immune cells. Additionally, owing to the limited number of patients with IBC included in our study, a larger clinical data set is needed to better understand the impact of AXL in IBC.

Conclusions

In conclusion, our study sheds light on the role of AXL signaling in regulating TAMs and maintaining an immunosuppressive TME in IBC, demonstrating that AXL is a significant therapeutic target in IBC and potentially other aggressive cancers.

Supplementary Information

The online version contains supplementary material available at <https://doi.org/10.1186/s13058-025-02015-8>.

Additional file 1.

Additional file 2.

Acknowledgements

We thank Sumitomo Pharma America, Inc., for providing the TP-0903 for our experiments. We are grateful to Cater Lee, her family, and The IBC Network Foundation for their fundraising efforts and continuous support for this project. We also thank Nalini B. Patel (MD Anderson Flow Cytometry and Cellular Imaging Core) for assistance with flow cytometric analysis and the MD Anderson Research Histology Core Laboratory for assistance with tumor histology. We thank Stephanie Deming and Don Norwood of Editing Services, Research Medical Library, MD Anderson Cancer Center, for editorial assistance. The proposed mechanism model was created using BioRender.

Author contributions

LTHP, YC, and YF contributed equally to this work. XW and NTU conceived the ideas and supervised the research. LTHP, YC, and YF performed most of the experiments. FB, PF, SJVL, and JL contributed to the data analysis. SK interpreted the staining data. All authors (LTHP, YC, YF, FB, PF, SJVL, FZ, JL, SO, SK, JMR, JMF, SLW, JMR, AKS, DT, NTU, and XW) discussed the results and revised the manuscript. All authors have read and approved the article.

Funding

This work was supported by U.S. Department of Defense grant W81XWH-21-1-0559 (to XW), an MD Anderson Institutional Research Grant (to XW), the Alligator's Hunt for Hope Adventure Fund (to XW), NIH grants 1R01CA205043-01A1 and 1R01CA258523-01A1 (to NTU), and Breast Cancer Research Foundation grants BCRF-23-164 and BCRF-24-164 (to NTU). Additionally, this research was supported by the NIH/NCI under award number P30CA016672, which supports the MD Anderson Advanced Technology Genomics Core and the MD Anderson Flow Cytometry and Cellular Imaging Core, and by the NIH/NCI under award number P30CA071789, which supports the University of Hawai'i Cancer Center Microscopy, Imaging, and Flow Cytometry Shared Resource.

Availability of data and materials

All data generated or analyzed during this study are included in this published article. Data regarding the RNA-sequencing experiment have been deposited at NCBI Sequence Read Archive database under BioProject accession number PRJNA1123282.

Declarations

Ethics approval

Animal experiments were approved by the MD Anderson Institutional Animal Care and Use Committee (protocol 00001072).

Consent for publication

Not applicable.

Competing interests

NTU holds consulting roles with AstraZeneca, Bayer, Pfizer, Gilead Sciences, Chugai Pharmaceutical, Daiichi Sankyo, Eisai Co., KeChow Pharma, Lavender Health, OBI Pharma, OncoCyte, Ourotech, DBA Pear Bio, Kirilys Therapeutics, Phoenix Molecular Designs, Preferred Medicine, Puma Biotechnology, Sumitomo Dainippon Pharma, Sysmex Co., Takeda Pharmaceuticals, CARNA Biosciences, ChemDiv, DualityBio, Oncolys BioPharma, Rakuten Medical, Merck, AnHeart Therapeutics, Carisma Therapeutics, and Eli Lilly. He also holds speaker or preceptorship roles with Bristol-Myers Squibb, Chugai Pharmaceutical, Genomic Health, Kyowa Hakkō Kirin Co., Sumitomo Dainippon Pharma, and Medscape. He also has research agreements in place with AnHeart Therapeutics, Eisai Co., Gilead Sciences, Phoenix Molecular Designs, Daiichi Sankyo, Puma Biotechnology, Merck, Oncolys BioPharma, OBI Pharma, ChemDiv, Tolero Pharmaceuticals, and VITRAC Therapeutics. AKS is a shareholder of BioPath and a consultant for Merck, AstraZeneca, Onxeo, ImmunoGen, Ivlon, GSK, and Kiyatec. DT receives funding for research (paid to MD Anderson Cancer Center) from Novartis and AMBRX. He receives consulting fees from AstraZeneca, OncoPep, GlaxoSmithKline, Gilead, Personalis, Sermonix, Pfizer, AMBRX, Novartis, Puma Biotechnology, Roche, Menarini, BeiGene, and Jazz Pharmaceuticals. AKS is a shareholder of BioPath and a consultant for Merck, AstraZeneca, Onxeo, ImmunoGen, Ivlon, GSK, and Kiyatec. DT receives funding for research (paid to MD Anderson Cancer Center) from Novartis and AMBRX. He receives consulting fees from

AstraZeneca, OncoPep, GlaxoSmithKline, Gilead, Personalis, Sermonix, Pfizer, AMBRX, Novartis, Puma Biotechnology, Roche, Menarini, BeiGene, and Jazz Pharmaceuticals.

Author details

¹Department of Breast Medical Oncology, The University of Texas MD Anderson Cancer Center, Houston, TX, USA. ²The University of Texas MD Anderson Cancer Center UTHHealth Houston Graduate School of Biomedical Sciences, Houston, TX, USA. ³Laboratoire d'Oncologie Prédictive, Centre de Recherche en Cancérologie de Marseille (CRCM), Inserm, U1068, CNRS UMR7258, Institut Paoli-Calmettes, Aix-Marseille Université, Marseille, France. ⁴Département d'Oncologie Médicale, Institut Paoli-Calmettes, Marseille, France. ⁵Center for Oncological Research (CORE), Integrated Personalized and Precision Oncology Network (IPPON), University of Antwerp, Universiteitsplein 1, 2610 Wilrijk, Belgium. ⁶Department of Biostatistics, The University of Texas MD Anderson Cancer Center, Houston, TX, USA. ⁷Cancer Biology Program, University of Hawai'i Cancer Center, Honolulu, HI, USA. ⁸University of Hawai'i Inflammatory Breast Cancer Clinic and Research Program, Honolulu, HI, USA. ⁹Department of Pathology, The University of Texas MD Anderson Cancer Center, Houston, TX, USA. ¹⁰Department of Hematopathology, The University of Texas MD Anderson Cancer Center, Houston, TX, USA. ¹¹Sumitomo Pharma America, Inc., Marlborough, MA, USA. ¹²Department of Medicine, University of California San Francisco, San Francisco, CA, USA. ¹³Department of Gynecologic Oncology and Reproductive Medicine, The University of Texas MD Anderson Cancer Center, Houston, TX, USA.

Received: 24 September 2024 Accepted: 3 April 2025

Published online: 06 May 2025

References

- Chang S, Parker SL, Pham T, Buzdar AU, Hursting SD. Inflammatory breast carcinoma incidence and survival: the surveillance, epidemiology, and end results program of the National Cancer Institute, 1975–1992. *Cancer*. 1998;82(12):2366–72.
- Hance KW, Anderson WF, Devesa SS, Young HA, Levine PH. Trends in inflammatory breast carcinoma incidence and survival: the surveillance, epidemiology, and end results program at the National Cancer Institute. *J Natl Cancer Inst*. 2005;97(13):966–75.
- Singh SR, Rameshwar P, Siegel P. Targeting tumor microenvironment in cancer therapy. *Cancer Lett*. 2016;380(1):203–4.
- Lim B, Woodward WA, Wang X, Reuben JM, Ueno NT. Inflammatory breast cancer biology: the tumour microenvironment is key. *Nat Rev Cancer*. 2018;18(8):485–99.
- Fu XT, Dai Z, Song K, Zhang ZJ, Zhou ZJ, Zhou SL, et al. Macrophage-secreted IL-8 induces epithelial-mesenchymal transition in hepatocellular carcinoma cells by activating the JAK2/STAT3/Snail pathway. *Int J Oncol*. 2015;46(2):587–96.
- Peranzoni E, Lemoine J, Vimeux L, Feuillet V, Barrin S, Kantari-Mimoun C, et al. Macrophages impede CD8 T cells from reaching tumor cells and limit the efficacy of anti-PD-1 treatment. *Proc Natl Acad Sci U S A*. 2018;115(17):E4041–50.
- Werno C, Menrad H, Weigert A, Dehne N, Goerdt S, Schledzewski K, et al. Knockout of HIF-1alpha in tumor-associated macrophages enhances M2 polarization and attenuates their pro-angiogenic responses. *Carcinogenesis*. 2010;31(10):1863–72.
- Song J, Liu Q, Han L, Song T, Huang S, Zhang X, et al. Hsa_circ_0009092/miR-665/NLK signaling axis suppresses colorectal cancer progression via recruiting TAMs in the tumor microenvironment. *J Exp Clin Cancer Res*. 2023;42(1):319.
- Mantovani A, Sozzani S, Locati M, Allavena P, Sica A. Macrophage polarization: tumor-associated macrophages as a paradigm for polarized M2 mononuclear phagocytes. *Trends Immunol*. 2002;23(11):549–55.
- Wolfe AR, Trenton NJ, Debeb BG, Larson R, Ruffell B, Chu K, et al. Mesenchymal stem cells and macrophages interact through IL-6 to promote inflammatory breast cancer in pre-clinical models. *Oncotarget*. 2016;7(50):82482–92.
- Valeta-Magara A, Gadi A, Volta V, Walters B, Arju R, Giashuddin S, et al. Inflammatory breast cancer promotes development of M2 tumor-associated macrophages and cancer mesenchymal cells through a complex chemokine network. *Cancer Res*. 2019;79(13):3360–71.
- Linger RM, Cohen RA, Cummings CT, Sather S, Migdall-Wilson J, Middleton DH, et al. Mer or Axl receptor tyrosine kinase inhibition promotes apoptosis, blocks growth and enhances chemosensitivity of human non-small cell lung cancer. *Oncogene*. 2013;32(29):3420–31.
- Asiedu MK, Beauchamp-Perez FD, Ingle JN, Behrens MD, Radisky DC, Knutson KL. AXL induces epithelial-to-mesenchymal transition and regulates the function of breast cancer stem cells. *Oncogene*. 2014;33(10):1316–24.
- Zhang G, Kong X, Wang M, Zhao H, Han S, Hu R, et al. AXL is a marker for epithelial-mesenchymal transition in esophageal squamous cell carcinoma. *Oncol Lett*. 2018;15(2):1900–6.
- Tanaka M, Siemann DW. Axl signaling is an important mediator of tumor angiogenesis. *Oncotarget*. 2019;10(30):2887–98.
- Taniguchi H, Yamada T, Wang R, Tanimura K, Adachi Y, Nishiyama A, et al. AXL confers intrinsic resistance to osimertinib and advances the emergence of tolerant cells. *Nat Commun*. 2019;10(1):259.
- Wu X, Zahari MS, Ma B, Liu R, Renuse S, Sahasrabudhe NA, et al. Global phosphotyrosine survey in triple-negative breast cancer reveals activation of multiple tyrosine kinase signaling pathways. *Oncotarget*. 2015;6(30):29143–60.
- Aveic S, Corallo D, Porcu E, Pantile M, Boso D, Zanon C, et al. TP-0903 inhibits neuroblastoma cell growth and enhances the sensitivity to conventional chemotherapy. *Eur J Pharmacol*. 2018;818:435–48.
- Patel V, Keating MJ, Wierda WG, Gandhi V. Preclinical combination of TP-0903, an AXL inhibitor and B-PAC-1, a procaspase-activating compound with ibrutinib in chronic lymphocytic leukemia. *Leuk Lymphoma*. 2016;57(6):1494–7.
- Wang X, Semba T, Phi LTH, Chaitnikun S, Iwase T, Lim B, Ueno NT. Targeting signaling pathways in inflammatory breast cancer. *Cancers (Basel)*. 2020;12(9):2479.
- Ye X, Li Y, Stawicki S, Couto S, Eastham-Anderson J, Kallop D, et al. An anti-Axl monoclonal antibody attenuates xenograft tumor growth and enhances the effect of multiple anticancer therapies. *Oncogene*. 2010;29(38):5254–64.
- Chiu KC, Lee CH, Liu SY, Chou YT, Huang RY, Huang SM, Shieh YS. Polarization of tumor-associated macrophages and Gas6/Axl signaling in oral squamous cell carcinoma. *Oral Oncol*. 2015;51(7):683–9.
- Yeh HW, Chiang CF, Chen PH, Su CC, Wu YC, Chou L, et al. Axl involved in mineral trioxide aggregate induces macrophage polarization. *J Endod*. 2018;44(10):1542–8.
- Klopp AH, Lacerda L, Gupta A, Debeb BG, Solley T, Li L, et al. Mesenchymal stem cells promote mammosphere formation and decrease E-cadherin in normal and malignant breast cells. *PLoS ONE*. 2010;5(8):e12180.
- Wang X, Saso H, Iwamoto T, Xia W, Gong Y, Puzsai L, et al. TIG1 promotes the development and progression of inflammatory breast cancer through activation of Axl kinase. *Cancer Res*. 2013;73(21):6516–25.
- Zhang D, LaFortune TA, Krishnamurthy S, Esteva FJ, Cristofanilli M, Liu P, et al. Epidermal growth factor receptor tyrosine kinase inhibitor reverses mesenchymal to epithelial phenotype and inhibits metastasis in inflammatory breast cancer. *Clin Cancer Res*. 2009;15(21):6639–48.
- Wang X, Semba T, Manyam GC, Wang J, Shao S, Bertucci F, et al. EGFR is a master switch between immunosuppressive and immunoactive tumor microenvironment in inflammatory breast cancer. *Sci Adv*. 2022;8(50):eabn7983.
- Charafe-Jauffret E, Ginestier C, Iovino F, Tarpin C, Diebel M, Esterni B, et al. Aldehyde dehydrogenase 1-positive cancer stem cells mediate metastasis and poor clinical outcome in inflammatory breast cancer. *Clin Cancer Res*. 2010;16(1):45–55.
- Berckelaer CV, Laere SV, Colpaert C, Bertucci F, Kockx M, Dirix LY, Dam PV. The immune micro-environment of inflammatory breast cancer is characterized by an influx of CD163+ tumor-associated macrophages. *J Clin Oncol*. 2022;40(16_suppl):2556.
- Zhang Q, Sioud M. Tumor-associated macrophage subsets: shaping polarization and targeting. *Int J Mol Sci*. 2023;24(8):7493.
- Martinez FO, Gordon S, Locati M, Mantovani A. Transcriptional profiling of the human monocyte-to-macrophage differentiation and polarization: new molecules and patterns of gene expression. *J Immunol*. 2006;177(10):7303–11.

32. Rahal OM, Wolfe AR, Mandal PK, Larson R, Tin S, Jimenez C, et al. Blocking Interleukin (IL)4- and IL13-mediated phosphorylation of STAT6 (Tyr641) decreases M2 polarization of macrophages and protects against macrophage-mediated radioresistance of inflammatory breast cancer. *Int J Radiat Oncol Biol Phys*. 2018;100(4):1034–43.
33. Larionova I, Kazakova E, Patysheva M, Kzhyshkowska J. Transcriptional, epigenetic and metabolic programming of tumor-associated macrophages. *Cancers*. 2020;12(6):1411.
34. Wu D, Liu X, Mu J, Yang J, Wu F, Zhou H. Therapeutic approaches targeting proteins in tumor-associated macrophages and their applications in cancers. *Biomolecules*. 2022;12(3):392.
35. Liu J, Geng X, Hou J, Wu G. New insights into M1/M2 macrophages: key modulators in cancer progression. *Cancer Cell Int*. 2021;21(1):389.
36. Junttila IS. Tuning the cytokine responses: an update on interleukin (IL)-4 and IL-13 receptor complexes. *Front Immunol*. 2018;9:888.
37. Samaniego R, Gutierrez-Gonzalez A, Gutierrez-Seijo A, Sanchez-Gregorio S, Garcia-Gimenez J, Mercader E, et al. CCL20 expression by tumor-associated macrophages predicts progression of human primary cutaneous melanoma. *Cancer Immunol Res*. 2018;6(3):267–75.
38. Qin R, Ren W, Ya G, Wang B, He J, Ren S, et al. Role of chemokines in the crosstalk between tumor and tumor-associated macrophages. *Clin Exp Med*. 2022;23(5):1359–73.
39. Munir MT, Kay MK, Kang MH, Rahman MM, Al-Harrasi A, Choudhury M, et al. Tumor-associated macrophages as multifaceted regulators of breast tumor growth. *Int J Mol Sci*. 2021;22(12):6526.
40. Kaplanov I, Carmi Y, Kornetsky R, Shemesh A, Shurin GV, Shurin MR, et al. Blocking IL-1beta reverses the immunosuppression in mouse breast cancer and synergizes with anti-PD-1 for tumor abrogation. *Proc Natl Acad Sci U S A*. 2019;116(4):1361–9.
41. Gratchev A, Kzhyshkowska J, Kannookadan S, Ochsenreiter M, Popova A, Yu X, et al. Activation of a TGF-beta-specific multistep gene expression program in mature macrophages requires glucocorticoid-mediated surface expression of TGF-beta receptor II. *J Immunol*. 2008;180(10):6553–65.
42. Liu Y, Zhou H, Zheng J, Zeng X, Yu W, Liu W, et al. Identification of immune-related prognostic biomarkers based on the tumor microenvironment in 20 malignant tumor types with poor prognosis. *Front Oncol*. 2020;10:1008.
43. Guedez L, Jensen-Taubman S, Bourbouli D, Kwityn CJ, Wei B, Caterina J, Stetler-Stevenson WG. TIMP-2 targets tumor-associated myeloid suppressor cells with effects in cancer immune dysfunction and angiogenesis. *J Immunother*. 2012;35(6):502–12.
44. Wiley SZ, Sriram K, Salmeron C, Insel PA. GPR68: an emerging drug target in cancer. *Int J Mol Sci*. 2019;20(3):559.
45. Gocher AM, Workman CJ, Vignali DAA. Interferon-gamma: teammate or opponent in the tumour microenvironment? *Nat Rev Immunol*. 2022;22(3):158–72.
46. Zhang M, Huang L, Ding G, Huang H, Cao G, Sun X, et al. Interferon gamma inhibits CXCL8-CXCR2 axis mediated tumor-associated macrophages tumor trafficking and enhances anti-PD1 efficacy in pancreatic cancer. *J Immunother Cancer*. 2020;8(1): e000308.
47. Pandey V, Fleming-Martinez A, Bastea L, Doeppler HR, Eisenhauer J, Le T, et al. CXCL10/CXCR3 signaling contributes to an inflammatory microenvironment and its blockade enhances progression of murine pancreatic precancerous lesions. *Elife*. 2021;10: e60646.
48. Makuch E, Jasyk I, Kula A, Lipinski T, Siednienko J. IFNbeta-induced CXCL10 chemokine expression is regulated by Pellino3 ligase in monocytes and macrophages. *Int J Mol Sci*. 2022;23(23):14915.
49. Zaidi MR, Merlino G. The two faces of interferon-gamma in cancer. *Clin Cancer Res*. 2011;17(19):6118–24.
50. Liu Z, Sun J, Gong T, Tang H, Shen Y, Liu C. The prognostic and immunological value of guanylate-binding proteins in lower-grade glioma: potential markers or not? *Front Genet*. 2021;12: 651348.
51. Lin Y, Xu J, Lan H. Tumor-associated macrophages in tumor metastasis: biological roles and clinical therapeutic applications. *J Hematol Oncol*. 2019;12(1):76.
52. Tan J, Xu T, Gou Y, Wang H, Liang Z, Cao Y, et al. CCL20/CCR6 axis mediates macrophages to promote proliferation and migration of ESCs by blocking autophagic flux in endometriosis. *Stem Cell Res Ther*. 2022;13(1):294.
53. Liu B, Jia Y, Ma J, Wu S, Jiang H, Cao Y, et al. Tumor-associated macrophage-derived CCL20 enhances the growth and metastasis of pancreatic cancer. *Acta Biochim Biophys Sin*. 2016;48(12):1067–74.
54. Lan Q, Lai W, Zeng Y, Liu L, Li S, Jin S, et al. CCL26 participates in the PRL-3-induced promotion of colorectal cancer invasion by stimulating tumor-associated macrophage infiltration. *Mol Cancer Ther*. 2018;17(1):276–89.
55. Hu K, Li SL, Gan YH, Wang CY, Yu GY. Epiregulin promotes migration and invasion of salivary adenoid cystic carcinoma cell line SACC-83 through activation of ERK and Akt. *Oral Oncol*. 2009;45(2):156–63.
56. Wang Y, Jing Y, Ding L, Zhang X, Song Y, Chen S, et al. Epiregulin reprograms cancer-associated fibroblasts and facilitates oral squamous cell carcinoma invasion via JAK2-STAT3 pathway. *J Exp Clin Cancer Res*. 2019;38(1):274.
57. Van Laere SJ, Ueno NT, Finetti P, Vermeulen P, Lucci A, Robertson FM, et al. Uncovering the molecular secrets of inflammatory breast cancer biology: an integrated analysis of three distinct affymetrix gene expression datasets. *Clin Cancer Res*. 2013;19(17):4685–96.
58. Jeong H, Hwang I, Kang SH, Shin HC, Kwon SY. Tumor-associated macrophages as potential prognostic biomarkers of invasive breast cancer. *J Breast Cancer*. 2019;22(1):38–51.
59. Qiu SQ, Waaijer SJH, Zwager MC, de Vries EGE, van der Vegt B, Schroder CP. Tumor-associated macrophages in breast cancer: Innocent bystander or important player? *Cancer Treat Rev*. 2018;70:178–89.
60. Gasper DJ, Tejera MM, Suresh M. CD4 T-cell memory generation and maintenance. *Crit Rev Immunol*. 2014;34(2):121–46.
61. Sun Y, Liu L, Fu Y, Liu Y, Gao X, Xia X, et al. Metabolic reprogramming involves in transition of activated/resting CD4(+) memory T cells and prognosis of gastric cancer. *Front Immunol*. 2023;14:1275461.
62. Wang H, Wu J, Ling R, Li F, Yang Q, He J, et al. Fibroblast-derived LPP as a biomarker for treatment response and therapeutic target in gastric cancer. *Mol Ther Oncolytics*. 2022;24:547–60.
63. Tang G, Yin W. Development of an immune infiltration-related prognostic scoring system based on the genomic landscape analysis of glioblastoma multiforme. *Front Oncol*. 2020;10:154.
64. Ji D, Song C, Li Y, Xia J, Wu Y, Jia J, et al. Combination of radiotherapy and suppression of Tregs enhances abscopal antitumor effect and inhibits metastasis in rectal cancer. *J Immunother Cancer*. 2020;8(2): e000826.
65. Liu R, Hu R, Zeng Y, Zhang W, Zhou HH. Tumour immune cell infiltration and survival after platinum-based chemotherapy in high-grade serous ovarian cancer subtypes: a gene expression-based computational study. *EBioMedicine*. 2020;51: 102602.
66. Xiao Z, Wang R, Wang X, Yang H, Dong J, He X, et al. Impaired function of dendritic cells within the tumor microenvironment. *Front Immunol*. 2023;14:1213629.
67. Szpor J, Streb J, Glajcar A, Fraczek P, Winiarska A, Tyrak KE, et al. Dendritic cells are associated with prognosis and survival in breast cancer. *Diagnostics*. 2021;11(4):702.
68. Gu-Trantien C, Loi S, Garaud S, Equeter C, Libin M, de Wind A, et al. CD4(+) follicular helper T cell infiltration predicts breast cancer survival. *J Clin Invest*. 2013;123(7):2873–92.
69. Linde N, Casanova-Acebes M, Sosa MS, Mortha A, Rahman A, Farias E, et al. Macrophages orchestrate breast cancer early dissemination and metastasis. *Nat Commun*. 2018;9(1):21.
70. Ramos RN, Missolo-Koussou Y, Gerber-Ferder Y, Bromley CP, Bugatti M, Núñez NG, et al. Tissue-resident FOLR2+ macrophages associate with CD8+ T cell infiltration in human breast cancer. *Cell*. 2022;185(7):1189–1207.e25. <https://doi.org/10.1016/j.cell.2022.02.021>.
71. Ray A, Hu KH, Kersten K, Courau T, Kuhn NF, Zaleta-Linares I, et al. Targeting CD206+ macrophages disrupts the establishment of a key antitumor immune axis. *J Exp Med*. 2025;222(1): e20240957.
72. Cheng S, Li Z, Gao R, Xing B, Yunong Gao Y, Yang SQ, et al. A pan-cancer single-cell transcriptional atlas of tumor infiltrating myeloid cells. *Cell*. 2021;184(3):792–809.e23. <https://doi.org/10.1016/j.cell.2021.01.010>.
73. Wu Q, Li X, Yang Y, Huang J, Yao M, Li J, et al. MICA+ Tumor cell upregulated macrophage-secreted MMP9 via PROS1-AXL axis to induce tumor immune escape in advanced hepatocellular carcinoma (HCC). *Cancers*. 2024;16(2):269.
74. Russell SM, Keegan AD, Harada N, Nakamura Y, Noguchi M, Leland P, et al. Interleukin-2 receptor gamma chain: a functional component of the interleukin-4 receptor. *Science*. 1993;262(5141):1880–3.

75. Conde P, Rodriguez M, van der Touw W, Jimenez A, Burns M, Miller J, et al. DC-SIGN(+) macrophages control the induction of transplantation tolerance. *Immunity*. 2015;42(6):1143–58.
76. Hu B, Wang Z, Zeng H, Qi Y, Chen Y, Wang T, et al. Blockade of DC-SIGN(+) tumor-associated macrophages reactivates antitumor immunity and improves immunotherapy in muscle-invasive bladder cancer. *Cancer Res*. 2020;80(8):1707–19.
77. Liu Y, Meng Y, Zhang T, Alachkar H. Dereglulation of apolipoprotein C2 gene in cancer: a potential metabolic vulnerability. *Clin Transl Med*. 2021;11(6): e406.
78. Shi S, Guo Y, Wang Q, Huang Y. Artificial neural network-based gene screening and immune cell infiltration analysis of osteosarcoma feature. *J Gene Med*. 2023;26(1): e3622.
79. Jian F, Yanhong J, Limeng W, Guoping N, Yiqing T, Hao L, Zhaoji P. TIMP2 is associated with prognosis and immune infiltrates of gastric and colon cancer. *Int Immunopharmacol*. 2022;110: 109008.
80. Cao L, Li W, Yang X, Zhang W, Li M, Zhang H, et al. Inhibition of host Ogr1 enhances effector CD8(+) T-cell function by modulating acidic microenvironment. *Cancer Gene Ther*. 2021;28(10–11):1213–24.
81. Mullbacher A, Lobigs M, Hla RT, Tran T, Stehle T, Simon MM. Antigen-dependent release of IFN-gamma by cytotoxic T cells up-regulates Fas on target cells and facilitates exocytosis-independent specific target cell lysis. *J Immunol*. 2002;169(1):145–50.
82. Strieter RM, Kunkel SL, Arenberg DA, Burdick MD, Polverini PJ. Interferon gamma-inducible protein 10 (IP-10), a member of the C-X-C chemokine family, is an inhibitor of angiogenesis. *Biochem Biophys Res Commun*. 1995;210(1):51–7.
83. Pages F, Berger A, Camus M, Sanchez-Cabo F, Costes A, Molidor R, et al. Effector memory T cells, early metastasis, and survival in colorectal cancer. *N Engl J Med*. 2005;353(25):2654–66.
84. Cheng WL, Feng PH, Lee KY, Chen KY, Sun WL, Van Hiep N, et al. The role of EREG/EGFR pathway in tumor progression. *Int J Mol Sci*. 2021;22(23):12828.
85. Hung CN, Chen M, DeArmond DT, Chiu CH, Limboy CA, Tan X, et al. AXL-initiated paracrine activation of pSTAT3 enhances mesenchymal and vasculogenic supportive features of tumor-associated macrophages. *Cell Rep*. 2023;42(9): 113067.

Publisher's Note

Springer Nature remains neutral with regard to jurisdictional claims in published maps and institutional affiliations.